SLAC-PUB-121
July 1965

PHYSICAL PROPERTIES OF FILAMENT WOUND GLASS EPOXY STRUCTURES AS APPLIED TO POSSIBLE USE IN LIQUID HYDROGEN BUBBLE CHAMBERS*

H. Brechna and W. Haldemann

Stanford Linear Accelerator Center, Stanford University, Stanford, California

ABSTRACT

The report describes physical property tests on glass filament-epoxy-film-composites which have recently been proposed as a feasible material for a liquid hydrogen bubble chamber body placed in a very high pulsed magnetic field. Static and dynamic loadings, dielectric strength, thermal conductivity, and permeability to liquids at various temperatures such as 300°, 77.8°, 28° and 4.2°K tests are performed on straight rectangular pieces of different composition at various thicknesses up to one inch and a series of cylinders up to 0.0362 inch wall thickness, up to failure stresses.

It is found that the physical properties of some of these composites are entirely suitable for liquid hydrogen bubble chamber use, namely at temperatures of 28°K and an internal pressure of 150 psi. Fatigue tests up to 10^7 cycles of operation up to 9000 psi flexural and 300 psi shear stress showed that the filament structure had not lost its original properties.

(Paper delivered at 1965 Cryogenic Engineering Conference, August 23-25, 1965, Rice University, Houston, Texas.)

*Work supported by U.S. Atomic Energy Commission

I. INTRODUCTION

The bubble chamber has established itself in high energy physics research as one of the most useful tools. Since 1952, after the first bubble chamber was introduced by Glaser,[1] hundreds of important experiments have been carried on successfully. With the increase of the energy of modern accelerators the need for better and larger bubble chambers has grown. Recent proposals to match the size and magnetic field to the particle energy[2] show an increase in the bubble chamber size up to 3.93m (14 feet). However, the magnetic field chosen was 20 kG, partly to save dc power which for the above proposal is about 11 MW.

In determining the bubble chamber's measurement accuracy, one has to consider the angle at the start of the track θ, from a vertex in the plane containing its original direction and the instantaneous radius of curvature of the track γ and the dip angle φ. With respect to the chamber plane the variations of these values are referred to as chamber errors.

Calculations carried on by Shutt[3] show that the optimum track length for measurements is:

$$L_{\theta opt} \simeq L_{p_{opt}} = 0.42 \cdot p^{0.66} \qquad (1)$$

with p the particle momentum in (MeV/c).

In order to achieve optimum measurement accuracy, the chamber length should be about 2-3 times L_{opt} for production and analysis of events. The existing bubble chambers are optimized for particle moments of $\sim$ 3 GeV/c or less and have a magnetic field of $\sim$ 20 kG, which is inadequate for higher particle energies.

New efforts may be seen toward higher magnetic fields, say 100 kG in a liquid hydrogen chamber length of about 1-2m to match 10 GeV/c particle momentum. These values seem adequate for liquid hydrogen chambers, but still insufficient for heavy liquid chambers.

The study of iron bound dc magnets shows that bubble chamber magnets for the above requirements have a power requirement of 57 - 300 megawatts, which is economically unsound.

New possibilities in large superconductive magnets for a 1-meter chamber may be feasible.[4] With the commercially available superconducting wires and ribbons such as Niobium Titanium or Niobium Tin, fields up to 100 kG may be achieved. The helium evaporation over the dewar to the ambient can be reduced by using an intermediate liquid hydrogen mantle around the liquid hydrogen jacket.

A third possibility is the use of a pulsed magnet. The pulse duration is matched to the operational time of the bubble chamber. Presently a few small pulsed bubble chamber magnets are in operation.[5,6,7] The heavy liquid bubble chamber built by the Max Planck Institute in Munich[5] has a coil inner diameter of 7 cm and a coil length of about 35 cm. Peak fields achieved in the chamber center exceeded 200 kG. Pulse duration is 10 ms and the repetition rate is from 10-100 sec. Energy required at the 10 kV level is about 3×10^5 joules with maximum of 3.5×10^5 amp peak current. 10-100 cal per pulse is dissipated as heat, which is also absorbed partly by the chamber body.

The only existing pulsed liquid hydrogen bubble chamber was built by the group working at the University of Birmingham.[6] The chamber has a diameter of 9 inches, the chamber body has a wall thickness of 0.1 inch

and the system of through illumination is used for flashing the chamber. The field pulse duration is two seconds, peak field 15 kG, and the pulse repetition rate one pulse per eight minutes. The magnet is energized from a motor generator set. Other pulsed magnets for use with heavy liquid bubble chambers built by the group at the Kurchatov Atomic Energy Institute, Moscow,[7] are mentioned here. Their largest chamber has a useful volume of 10 liters and with a field of 10 kG, pulse duration 25 ms, and the other chamber has a diameter of 7 cm, a length of 4 cm, and operates at 60 kG. Both magnets are energized from capacitor banks rated 9×10^4 joules and 7.3×10^4 joules.

The required peak energy to pulse a 100 kG magnet with a bore of 1.3 m and a length of 0.5 m is 95×10^6 joules and the use of capacitor banks is not recommended. However, it is feasible to use homopolar generators in combination with asynchron motors and flywheels.

Since the technology with this pulse system has been practiced extensively, it was considered worthwhile to explore such a combination with a pulsed magnet for a liquid hydrogen bubble chamber. However, at pulse durations of 3-5 seconds and a repetition rate of one (1) pulse per 20 seconds, the eddy current heating makes a metal chamber body impractical and the use of a non-metallic chamber had to be explored.

The chamber operation is restricted to piston expansion system. Bellows were eliminated due to the fact that non-metallic Ω bellows for cryogenic use are presently unavailable. The use of gas expansion was found to be cumbersome and is therefore omitted.

The recent advancements in structural vessel design[8,9,10] were studied in detail as a prime candidate to be used for bubble chamber

design. The advantages of a structural bubble chamber are the low weight, the low thermal loss factor, elimination of eddy current losses for fast or slow pulses, and the very attractive static and dynamic properties discussed in Section IV.

However, the application of a structural material in combination with a liquid hydrogen bubble chamber made a new chamber and magnet design, as well as a thorough understanding of the fatique properties, permeability to cryogenic liquids, thermal properties and reliability of glass filament structures, imperative.

II. PULSED MAGNET

The basic idea in building a pulsed bubble chamber magnet is to match the field pulse duration to the chamber operational cycle. The total energy required for producing the magnetic field of 100 kG in the center of the bubble chamber is calculated from

$$E = E_f + E_e + Q \tag{2}$$

where:

The field energy is space

$$E_f = \int \frac{B^2}{2\mu_o} dV \tag{3}$$

The field energy is in the skin layer of a metallic bubble chamber

$$E_e = \oint \frac{B_n^2}{2\mu_o} \cdot \frac{\delta_n}{2} \cdot dA \tag{4}$$

and due to ohmic losses

$$Q = 2\pi(\alpha^2-1)\ \beta\lambda\ a_1^3 \int \rho J^2 dt + Q_{F_e} \qquad (5)$$

Though the procurement of the magnet itself does not produce many difficulties, the use of a fast pulsing capacitor bank makes the project unsatisfactory.

A circuit of CLR is efficient when the applied voltage to the magnet terminals is several kilovolts. On the other hand, a study of different coolants (LH_2, LN_2 and H_2O) shows that the most efficient cooling medium would be high purity water with a resistivity of $\rho > 5 \times 10^5$ ohm·cm. The magnet coil must be designed for high voltage application and the insulation problems may jeopardize the reliability of the magnet. A better scheme is to apply a pulse of several seconds to the magnet terminals with a repetition rate of 10 seconds or more between pulses. The oscillogram of such a pulse is shown in Fig. 1. The operational time of the bubble chamber varies between 17 and 30 ms, and if the constant field duration is chosen to be one second the chamber can be operated 10 times during one pulse. The average duty cycle of the magnet would be 1 pulse per twenty (20) seconds, and of the chamber one (1) pulse per two (2) seconds.

The existing methods of taking pictures are not able to photograph 10 times per second. However, occuring events may be photographed during each pulse.

By using the pulsing scheme shown in Fig. 1, the magnet is designed for a low voltage of 80 volts, a current of 1.3×10^6 amps and a peak energy of 95×10^6 joules. The coil consists of 12 turns connected in series. A simplified cross section of the magnet is shown in Fig. 2. The important magnet data are given in Table I.

TABLE I

DATA FOR VARIOUS 100 kG MAGNET TYPES

		Water cooled dc Magnet	Superconducting Magnet	Water cooled Pulsed Magnet
Coil inner diameter $2a_1$	(cm)	137	137	137
Coil outer diameter $2a_1\alpha$	(cm)	410	240	206
Axial gap width $2a_1\beta g$	(cm)	36	36	36
Left coil length $2a_1\beta_1$	(cm)	60	22	22
Right coil length $2a_1\beta_2$	(cm)	120	40	50
Left coil center position	(cm)	-48	-29	-29
Right coil center position	(cm)	+78	+38	+43
Maximum ampere turns	(Amp)	21.4×10^6	17×10^6	15×10^6
Total number of turns		476	18×10^3	12
Peak voltage (coils in series)	(Volt)	1.27×10^3	---	80
Peak current (coils in series)	(Amp)	4.5×10^4	700	$1.3 \times 10^6 \pm 1\%$
Coil resistance (90°C)	(Ohm)	2.8×10^{-2}	---	60×10^{-6}
Dc power (peak)	(Watts)	57×10^6	---	102×10^6
Peak energy	(joules)	161×10^6	110×10^6	95×10^6
Pulse duration	(sec)	---	---	4
Pulse repetition rate	(sec^{-1})	---	---	20
r.m.s. power (15% recovery)	(Watts)	---	---	10.2×10^6
Amount cooling water	(G.p.m.)	4420	---	795
Radial stress	(kp/cm^2)	406	406	406
Maximum shear stress	(kp/cm^2)	460	703	703
Coil weight	(kg)	128×10^3	3×10^3	12×10^3
Weight of iron shell	(kg)	1100×10^3	1000×10^3	360×10^3
Structural support	(kg)	40×10^3	40×10^3	50×10^3

The eddy current losses in a stainless steel chamber, non-uniformly distributed, is for our particular case with 4.0-sec pulse duration, 950 watts...exceeds substantially the already existing static heat losses from the stainless steel body over superinsulation to the ambient (~ 300 watts for a 500-liter liquid hydrogen chamber) and the dynamic losses (~ 250 watts for 1 pulse/2 sec) due to the piston movements.

From previous experiments[8,9] it was known that glass filament-epoxy structures used for rockets and missiles have excellent static cryogenic properties. For a structural bubble chamber body (Fig. 3) the dynamic losses are reduced to frictional losses between the neck and the piston and the dynamic losses in the liquid hydrogen (~ 80 watts for 1 pulse per 2 sec average operation), and to static losses to ambient of 150 watts.

To obtain peak power in excess of 100×10^6 watts for one second the following schemes were studied:

a. Homopolar generators driven by induction motors and flywheels.

b. Ac generators driven by induction motors and flywheels with controlled rectifiers for dc output.

c. Energy storage by means of capacitors or inductors.

The first mentioned method seemed to be the most promising from the point of view of initial cost and ease of operation. The effect of fast field pulsing on liquid hydrogen in the chamber is not well known. Bergmann[5] mentions formation of large bubbles during pulsing.

Slow pulses do not show the same effects in liquids. Using the pulse diagram (Fig. 1) and data of Table I we obtain an rms power of 10.2 megawatts, at an operational cost of $204,000 per year (2000 hours of operation).

The schematic diagram of the magnet and energizing system is shown in Fig. 4. The cost breakdown of the system is given in Table II, compared to the costs of a 100 kG dc and a 100 kG superconducting magnet.

TABLE II

CAPITAL AND OPERATIONAL COST OF DIFFERENT MAGNET TYPES*

Capital Cost	Water cooled d.c. Magnet	Superconducting Magnet	Water cooled Pulsed Magnet
1. Magnet Coil	$ 0.73 × 10^6	$ 3.6 × 10^6	$ 0.090 × 10^6
2. Iron Yoke	1.74 × 10^6	1.6 × 10^6	0.95 × 10^6
3. Coil Connections	0.09 × 10^6	0.08 × 10^6	0.06 × 10^6
4. Bus Connections to Power Supply	0.03 × 10^6	---	0.04 × 10^6
5. Dewars, Transfer lines, etc.	---	0.15 × 10^6	---
6. Power Supply			
a. Inst.	1.80 × 10^6	---	---
b.	---	0.007 × 10^6	---
c.	---	---	4.0 × 10^6
7. Water pumps, Cooling tower and Controls	0.2 × 10^6	---	0.17 × 10^6
8. Instrumentation	0.05 × 10^6	0.12 × 10^6	0.05 × 10^6
9. Miscellaneous	0.12 × 10^6	0.15 × 10^6	0.12 × 10^6
TOTAL CAPITAL COST	$ 4.76 × 10^6	$ 5.707 × 10^6	$ 5.48 × 10^6
Escalation and Contingency (15%)	$ 0.715 × 10^6	$ 0.855 × 10^6	$ 0.822 × 10^6
Operational Cost			
10 years, 2000 hours/year** (Power)	$ 11.4 × 10^6	$ ---	$ 2.04 × 10^6
Liquid Helium***		1.9 × 10^6	
Liquid Hydrogen		0.3 × 10^6	
Liquid Nitrogen		0.05 × 10^6	
Maintenance	0.15 × 10^6	0.4 × 10^6	0.3 × 10^6
TOTAL OPERATIONAL COST	$ 11.55 × 10^6	$ 2.65 × 10^6	$ 2.34 × 10^6

* No coil damage and part replacement included

** $\$10^{-2}$/kWh power price

*** 7 - 10 cool downs per year

III. BUBBLE CHAMBER PARAMETERS

Due to eddy current losses in all metallic parts within the high magnetic field region and the requirement of a temperature gradient of 5×10^{-2} °K over the entire liquid hydrogen volume, the bubble chamber, and auxiliary parts exposed to the pulsed field and in contact with the liquid hydrogen must be built from non-metallic parts. The internal pressure of the chamber changes during expansion and recompression from ~ 90-45 psi (6.4-3.2 kg/cm^2) and due to mechanical stress requirements on the chamber, the shape of the chamber is partly predetermined. The stress distribution over the chamber walls is calculated for the 1 meter bubble chamber with a wall thickness of 1.25 inch and an internal pressure of 150 psi which is shown in Fig. 3b and 3c. The maximum longitudinal and circumferential stress at the chamber wall is lower than 3000 psi. The investigation of materials to fit in this particular application led to the choice of high tensile glass fibers (S/HTS) in combination with high purity epoxies.

The bubble chamber (Fig. 3a) consists of S-HTS glass roving in a matrix composed of Union Carbide ERL 2256 epoxy and the MPDA hardener. The structure has a resin content of ~ 20 percent by weight. The wall thickness of the chamber was chosen to be approximately 1.25 inches in order to reduce chamber body distortion during operation to a minimum and provide ample safety. To reduce permeability to liquid hydrogen, two sheets of H-film were incorporated into the chamber structure. The chamber beam entrance window must be of low Z material and therefore either a sheet of pure beryllium, stainless steel or the glass filament structure itself but of much lesser thickness than the chamber wall may be used. The window shape, inwardly convex, is dictated by the internal

chamber pressure during operation. It is difficult to fabricate the transition region from the chamber to the expansion neck with HTS-roving and due to the relatively small stresses in the chamber, glass fiber cloth may be used. The shape of the dome is mainly due to shear stress limitations in the glass filament structure. The chamber optical window is pressed to the bubble chamber axially by means of another filament structure cylinder and the pressure is applied externally to both the radiation shield and the internal pressure ring. Conventional inflatable gaskets are used to force the ring against the window and Kel-F-81 is proposed to seal the chamber.

Since recompression of bubbles produces heat, unnecessary bubble formation should be avoided and the number of spontaneous bubbles at the walls should be kept to a minimum by using fairly smooth wall surfaces. By using collapsible polished stainless steel cores, the inner wall surface of glass filament structures can be made very smooth. An alternate solution to use Mylar liners in the inside of the bubble chamber walls can be considered.

Cooling ducts are provided to the chamber body by means of cavities. In order to reduce the static heat loss to the ambient, multi-layers of superinsulation will be used to fill a 0.5 inch radial space around the chamber. Each layer of superinsulation is additionally insulated to prevent short circuits between aluminum layers applied to the mylar film. The heat loss calculated in the superinsulation due to the pulse field is 30 watts. The weight of the bubble chamber including neck is 410 kg and the weight of the total magnet, vacuum tank and bubble chamber complex is 450×10^3 kg.

The expansion system is fast acting, but of a conventional piston type gadget. The chamber control panel is conventional; however, all the piping below the neck is made from the filament glass-epoxy structure.

The vacuum tank and accessory parts are built from type 304 stainless steel and the induced heat due to eddy current is removed by means of water cooling. Cooling tubes are brazed on the tank walls.

From tests conducted on flat bar samples it became evident that the main cause of failure in the filament matrix was a 6000 psi rms value of interlaminar shear stress at 28°K (see Section IV). The particular bubble chamber design in Figs. 3a and 3c would have an interlaminar shear stress of 400 psi and the design of 3b a shear stress of 300 psi, both at a 150 psi internal pressure. Fatigue tests with 300 psi shear stress did not reveal any drop in the structure strength. Calculations are based on a Poisson ratio of 0.25 (for glass roving).

The cylindrical body stresses (Figs. 3b and 3c) at the transition point with the elliptical dome include the effect of the head. The ellipitical head stresses are calculated for an ellipsoid of revolution[11,12] and the effect of the mating cylindrical section is absent. The elliptical head stresses should be modified adjacent to the transition point to agree with the cylindrical section stresses.

Static and dynamic tests on filament structures at different cryogenic temperatures were carried on specifically to test the reliability of the filament to be used in a large liquid hydrogen bubble chamber. The stresses are derived from the internal chamber pressures and the fatigue tests are related to the actual values on the wall. The longitudinal and circumferential stresses on the chamber wall are about 5.1% of the ultimate flexural strength of the glass filament epoxy complex (55,000 psi) and about 6.7% of the ultimate shear stress of 6000 psi.

IV. TEST PARAMETERS

Scope

The main objectives of testing glass filament structures to be used in bubble chambers are reliability, thermodynamic properties and fatigue behavior at liquid hydrogen temperature. With an average duty cycle of one chamber operation every two seconds, the total operation over ten years is 3.6×10^7 at an internal pressure of 150 psig maximum. The tests performed on filament structures were basically the final choice of the epoxy, glass filament matrix, the testing of the ultimate flexural and shear strength, fatigue properties, the thermal conductivity and the dielectric constant, and the permeability to cryogenic liquids.

In order to make a final decision in the choice of the proper epoxy to be used in the filament structure, different epoxies (see Table III) were tested and the final choice was ERL 2256 (Union Carbide) and the hardener MPDA (DuPont).* The resin content of the structure fluctuated between 21-25 ppw. The samples to be tested were chosen straight 1-inch wide and 6-10 inches long with different thicknesses from 0.125-1 inch in order to obtain relative values.

The maximum flexural stress was determined by delamination of the composite due to shear stresses. Final tests with filament wound cylinders were performed in order to measure composite stresses and to confirm tests performed on straight samples.

---

*Samples provided by United Technology Center (UTC), Sunnyvale, Calif.

TABLE III

SAMPLE DESIGN AND PROPERTIES (ANISOTROPIC CONDITION)

SAMPLE SERIES:		1	2	3	4	5	6
Reinforcement		S-HTS roving	S-HTS roving	S-HTS roving	2P-143 S-HTS Glass Cloth	S-HTS roving	S-HTS roving
Resin		ERL 2256 Epoxy (Union Carbide)	DER 332 Epoxy (Dow Chem.Co)	DER 332	ERL 2256	DER 332	ERL 2256
Hardener (parts/100 resin)		MPDA (19.2)	MNA (45) BDMA (.5)	MNA (45) BDMA (.5)	MPDA (19.2)	BF_3 MEA (3)	MDA (19.2)
Cure Cycle		4h. at 145°C	4 h. at 177°C	4 h.at 177°C 1 h.at 232°C	4 h.at 145°C	4 h.at 145°C	4 h.at 145°C
Sample Construction	L	1 layer at 554 e/inch 4 layers at 462 e/inch	5 layers at 480 e/inch		18 layers warp 8 layers fill	5 layers at 480 e/inch	
	H	2 layers at 554 e/inch 8 layers at 462 e/inch	10 layers at 480 e/inch		8 layers warp 18 layers fill	10 layers at 480 e/inch	
Sample Dimensions		6x1x0.25 in.	6x1x0.272 in.	6x1x0.272 in.	6x1x0.257 in.	6x1x0.243 in.	6x1x0.243 in.
Span length		5 inches	5 inches	5 inches	5 inches	5 inches	5 inches
Resin content							
by weight %		21.5	20	20	31	20	19
by volume %		37	34	34	46	34	33

TABLE III - Continued

SAMPLE DESIGN AND PROPERTIES (ANISOTROPIC CONDITION)

SAMPLE SERIES:	1	2	3	4	5	6
Ultimate Flex.	1.76×10^5	- *)	- *)	1.32×10^5	- *)	1.94×10^5
$300^{\circ}K$ (psi)	1.76×10^5	- *)	- *)	1.32×10^5	- *)	1.94×10^5
Flex. Mod.						
$300^{\circ}K$ (psi)	7.3×10^6	- *)	- *)	5×10^5	- *)	7.4×10^6
Elongation						
$300^{\circ}K$ (psi) (inch/inch)	0.027	- *)	- *)	0.025	- *)	0.0268

*) Samples delaminated at ~ 10^5 psi flexural stress.

The test apparatus for the flexural stress is shown in Fig. 5a and the detail configuration of the breaker in Fig. 5b. The deflection-load curve was taken by means of a recording oscillograph and the load is provided by means of a 10^4 lbs. load cell.

The fatigue tester shown in Figs. 6a and 6b vibrate the sample at 5 cps with a preset load. Samples and their clamping system can be placed in 8-inch liquid helium dewars and the samples may be broken in the liquid desired for testing. The thermal conductivity tests were performed with cylindrical samples where HTS glass roving was wound tightly around a stainless steel tubing, the thermoset applied on each glass layer. The samples were insulated thermally on both ends from the bath. The samples were cooled down at the start of the experiment with $5^{\circ}K$/hour and after the evidence was provided that the cool down did not effect the mechanical strength appreciably the cool down rate was increased to about $150^{\circ}K$ per hour average. It was also found that samples with thin layers of glass (Fig. 7) had no hysterisis after several shock cool-downs and warm-ups, and that the mechanical strength of straight samples of identical overall dimensions with thicker longitudinal layers ($\sim$ 0.1") was 35% lower than samples with thin longitudinal layers (0.035") and that both flat surface-layers showed cracks due to cool-down, even if the cool-down rate was kept below $5^{\circ}K$/hour. The ratio of longitudinal (L) to cross-over (H) layer thickness is 2:1; the number of ends per inch longitudinal (L) layer is 462-554.

The tests performed on straight samples are sensitive to which flat surface the pressure from the ram head should be applied. Test values vary between 15-18%. This effect is due purely to manufacturing problems and for comparative testing the surface effect must be guarded carefully.

For testing straight samples, the ASTM D790 Standards, with a single pressure finger of r = 0.1875 inch radius could not be applied. Due to the high flexural strength of the samples, the top layers in close contact with the ram head were broken under the test finger which lead to 20-23% lower values of E modulous and shear strength, and therefore to wrong conclusions.

The 0.25-1 inch samples were tested with a double pointed ram head, r = 0.25 inch finger radius, one inch apart, and the 0.125 inch thick samples were tested with a single pointed ram head. The double pointed ram head gave a constant bending moment over one inch of the sample length, and therefore a more uniformly distributed load.

Static Tests with Straight Samples

The flexural and shear strength of various samples versus sample thickness at different temperatures with a different mode of construction calculated for isotropic specimen are given in Figs. 8 and 9. The points shown are rms values from 3-9 samples tested.

The liquids chosen for testing were liquid nitrogen and liquid helium. The test data at liquid hydrogen temperature are obtained by cooling the samples with cold helium gas.

Samples delaminate first and then break at ultimate shear strength, rather than flexural strength. The ultimate flexural strength values are dictated by the maximum shear strength. The use of film barriers in the

HTS-glass-epoxy structure shows a weakening of the matrix, when Mylar, Tedlar and Beryllium film layers were used, but changed negligibly when H-film was incorporated.

In the case of Mylar, Tedlar and Beryllium sheets, each 0.002 inch thick, located at the neutral axis and 0.020 inch inside the top surface, the shear strength was reduced from 39-34% at room temperature, 72-42% at 77.8°K, and 73-45% at 4.2°K, compared to samples without film barriers.

Using medium weave HTS-glass fiber cloth the ultimate shear strength was 40% (at 77.8°K) and 34.4% (at 4.2°K) lower compared to unidirectional samples.

Film barriers made of 0.002 inch thick H-film showed a reduction of 3-5% of the ultimate shear strength of pure glass-epoxy filament structures.

The calculation of the ultimate shear and flexural strength of filament structures were based on the assumption that the cross-over (H) layers do not contribute to the strength of the sample. This anisotropic specimen calculation leads to higher values of flexural strength and elastic modulus, but does not effect the shear strength calculations. The equation used for obtaining the ultimate shear and flexural stress values are the well known equations for isotropic specimen. Where tension and compression moduli are identical, however, the equations for elastic modulus and maximum fiber strain for one and two point loading for 2 and 5 inch spans are repeated in Eqs. (6) and (7) for reference:

$$E = 0.167 \frac{W}{\delta I} \qquad (6a) \qquad \text{one point load}$$

$$E = 2.33 \frac{W}{\delta I} \qquad (6b) \qquad \text{two point load}$$

$$e = 1.5\ t\delta \qquad (7a) \qquad \text{one point load}$$

$$e = 0.214\ t\delta \qquad (7b) \qquad \text{two point load}$$

With t = section thickness and δ = measured ram head motion (inch)

I = cross-sectional moment of inertia with respect to the neutral axis

W = applied load in pounds

The maximum fiber strain is less than 5% and the Eqs. (6) and (7) applicable. Maximum deviations are occuring in the range of 77.8°K - 300°K. The changes are reduced at lower temperatures. Figures 10 and 11 illustrate E-modulus as a function of the sample thickness and the shear strength for 0.25 inch thick samples with different design parameters as functions of the bath temperature.

Dynamic Tests with Straight Samples

Fatigue tests performed on straight samples were comparable to stresses occuring in the bubble chamber body. The maximum flexural stresses were therefore chosen $\pm 3 \times 10^3$, $\pm 6 \times 10^3$, and $\pm 9 \times 10^3$ psi compared to an expected maximum longitudinal and circumferential stress in the chamber of 2,800 psi and shear stress of 300 psi at an internal pressure of 150 psi. From static tests the relative properties of the filament structure at various cryogenic temperatures are known. From reasons of simplicity, fatigue tests at 77.8°K were chosen. Sample thickness for all tests is 0.25 inch. Table IV gives the result of the fatigue testing. The samples were broken after the fatigue cycle at liquid nitrogen temperature. No practical deviation from original values obtained from static tests could be observed.

Thermal Cycle Tests

To study the effect of fast cool-downs of filament structures, 0.25 inch and 0.5 inch samples were shock cooled and warmed up repeatedly. Samples with 0.035-inch thick layers (with 554 ends per inch) did not show

TABLE IV

UNIDIRECTIONAL FATIGUE TESTS ON FLAT SPECIMEN

Sample Structure	Max. Flex.Stress PSI	Max. Defl. Inches	Fatigue Test Temperature	Number of Cycles	Deviation from Original Value
HTS - Filament Structure (No film barrier)	± 3000	± 0.024	77.8°K	5×10^6	None
HTS - Filament Epoxy Structure with H-Film Barriers	± 3000	± 0.024	77.8°K	10×10^6	None
HTS - Filament Epoxy Structure with H-Film Barriers	± 6000	± 0.058	77.8°K	16.7×10^6	None
HTS - Filament Epoxy Structure with H-Film Barriers	± 9000	± 0.089	77.8°K	4×10^6	None
HTS - Glass cloth-epoxy Structure (No film barrier)	± 3000	± 0.024	77.8°K	6.5×10^6	None

any significant changes in shear and flexural strength after 15 cycles. Samples with 0.1 inch thick layers (554 ends per inch) showed a 31% reduction in shear strength after one (1) cycle.

Stressed and Unstressed - Low Temperature Permeability Test

Glass filament epoxy structures are permeable to liquids.[13] The penetration depth of high purity water in glass filament epoxy structures at ambient temperature and atmospheric pressure is 0.05-0.1 cm in 20 days. At liquid hydrogen temperature the situation changes as follows: The filament structure becomes less permeable at temperatures of 28 °K and lower. Due to the fluidity of liquid hydrogen the diffusion in the filament structure is enhanced.

In order to reduce the permeability of the filament epoxy matrix such that small leaks may be pumped out, film barriers, such as 0.002 inch of Mylar, Tedlar and H-film, had been incorporated in the filament structure body.[14] The specimen to be tested had a thickness of 0.25 inch and a diameter of about 6 inches. It was placed in a cell comprised of two demountable stainless steel flanges, each with a cavity of 1.57 cubic inches. The specimen were clamped between the two flanges and acted as a divider separating the cavities. The air was evacuated from one cavity and gaseous helium was pumped in with a pressure of 150 psi into the other cavity. The evacuated cavity is connected with a CEC mass spectrometer leak detector, model 24-120B.

From previous tests performed at ambient temperatures by J. M. Toth with 0.002 inch of Mylar and Tedlar, and 0.001 inch of H-film it was known that polymeric films are permeable to liquids. However in glass filament epoxy structures with H-film barriers, after reaching equilibrium no leaks larger than $10^{-9} \frac{kg}{cm^2} \times cm^3/sec \cdot cm^2 \cdot cm$ could be measured after 72 hours at ambient and at 77.8°K.

Heat Conductivity

The radial heat flow method was selected for this experiment in order to minimize heat leaks. The specimen used consists of a 0.75 inch stainless steel tubing, wrapped with S-994/HTS glass filament and epoxy, specified in Table III. The inner stainless steel tubing is heated by means of a constant current dc power supply and the voltage drop across the tubing is measured continuously. Copper-constantan thermocouples were located in the filament structure as shown in Fig. 12. The end part of the tube was thermally insulated in order to force the heat to pass radially through the filament structure.

Transformer oil, liquid nitrogen and liquid helium were used as a constant temperature both to maintain a fixed outside wall temperature on the specimen to be tested.

In steady state condition the thermal conductivity in radial direction may be obtained from Eq. (8):

$$k_m = \frac{P_o \ln(r_i/r_{i-1})}{2\pi L \Delta \theta} \left(\frac{W}{cm^oK}\right) \qquad (8)$$

with L the length of specimen in cm, P the input power in watts and $\Delta\theta$ the temperature drop across the filament epoxy matrix in ^oK. Figure 12 gives the measured values of k_m versus the bath temperature. Values measured are higher than the data given in lit. cit.[15] but it is believed that the compact void free structure does mostly account for it.

Biaxial Stresses

Mechanical property tests were made at 303^oK and 77.8^oK with the UTC built biaxial cylinders shown in Fig. 13a. The cylinders permit evaluation of stresses of the glass epoxy structure under conditions of actual use

in bubble chambers. The cylinders have a 3-inch inside diameter, a length of 6.25 inches, and a wall thickness of 0.0362 inch. Twelve-end S994/HTS glass fibers and Union Carbide ERL 2256/MPDA resin were used in the construction. The resin content is 19-20% by weight and the cross sectional area of the filament is 21.93×10^{-6} square inches. The thickness of a helical layer is 0.0105 inch for a structure equally strong in hoop and longitudinal directions. A layer of DuPont "H667" film was applied at approximately half the wall thickness. A 45° winding angle was used and hoop passes were applied to obtain the balanced structure.

Ultimate burst pressure calculated at room temperature was 2294 psi and 3130 psi which corresponds to a glass failure stress of 250,000 psi at $700^{\circ}K$. At $300^{\circ}K$ the ultimate burst pressure measured was 2400 $\pm$ 5% psi, corresponding to a glass failure stress of 262,000 psi. In order to obtain strain values versus applied pressure strain-gages were fixed on the cylinder surface inside the top filament layer. Strain values as a function of hoop stress is shown in Fig. 14.

Thermal Contraction

Thermal contraction tests with glass filament epoxy structures simulating the actual behavior of the cylindrical bubble chamber were made in the temperature range of $4.2^{\circ}K$ to $302^{\circ}K$ by using straight bars with a balanced structure. The tests samples (S994/HTS glass roving with 19% by weight epoxy content) have an average density of 2.1 $gr \cdot cm^{-3}$. The thermal contractions of the samples are mainly dictated by the glass filaments. The test data are given in Fig. 15 and the results may be compared with values obtained for H-film from measurements reported by J. M. Toth.[9]

Dielectric Strength

A 15kV, 60 cps, SLAC-designed corona measuring device and a 100 kV power supply were used to determine the corona threshold values and the dielectric strength of filament-epoxy structures. Rogovsky type electrodes (0.5 inch diameter) were used for testing. One electrode is stationary and the other could be adjusted by spring loading to the required pressure. The samples, about 6-inches in diameter and 0.1 $\pm$ 0.005 cm thick and a H-film barrier of 0.005 cm were made in the same way, as the 3-inch ID cylinders. They were placed between the electrodes and the voltage applied to one electrode was increased in increments of 100 volts until breakdown. The dielectric strength of the samples in air is 48 $\pm$ 13% kV/mm, at liquid nitrogen 60 $\pm$ 9% kV/mm and at liquid helium 45 $\pm$ 11% kV/mm were measured. The corona threshold measured were:

6.5 kV/mm in air at ambient temperature of 298°K

9.8 kV/mm at 77.8°K immersed in liquid nitrogen bath

8.3 kV/mm at 4.2°K immersed in liquid helium bath.

S994 high strength glass fiber cloth epoxy structures were tested in the same manner as above for unidirectional samples and due to poor impregnation a breakdown voltage of 13 $\pm$ 50% kV/mm of air and 40 kV $\pm$ 7% of liquid nitrogen was measured.

V. SUMMARY OF RESULTS AND CONCLUSIONS

The study results and the evaluation of the test data for glass-filament epoxy structures exposed to cryogenic temperatures, particularly to liquid hydrogen, show that glass filament structures are equivalent to stainless steel chambers with dc field operation and superior to a stainless steel bubble chamber exposed to a transient magnetic field.

The advance in knowledge in the static and dynamic behavior makes the filament wound chamber attractive. However, a number of problems such as the feed through tubing to the chamber, the safety problems usual in any bubble chamber, the sealing of the chamber, and the properties of liquid hydrogen exposed to pulsed fields must be investigated further in detail. In addition to the important feature of the low weight chamber (compared to the stainless steel body), the static heat loss of the glass filament structure is considerably less and the structure is reliable for bubble chamber operations.

Acknowledgments

The authors would like to thank Mr. J. A. Anderson, SLAC, who performed most of the chamber stress calculations, Mr. J. Hegis, SLAC, for cooperation in the measurements, Mr. W. A. Porter, United Technology Center, who built the samples, and Mr. R. Mizrahi, SLAC for the studies of the energizing system.

REFERENCES

1. D. A. Glaser, Phys. Rev. 87, 665 (1952).
2. M. Derrick, et al., "Proposal for the Construction of a 12-Foot Hydrogen Bubble Chamber," Argonne National Laboratory (June 10, 1964).
3. R. P. Shutt, "Recent Advances in the Bubble Chamber Technique," Nucl. Instr. and Methods 20 (1963).
4. C. Laverick and G. Lobell, "Large High Field Superconducting Magnet System," Rev. Sci. Instr. 36, No. 6 (1965).
5. W. H. Bergmann, et al., "High Field Bubble Chamber," Nucl. Instr. and Methods 20, No. 1 (1963).
6. D. C. Colley, et al., "9-inch Liquid Hydrogen Bubble Chamber in a Pulsed Magnetic Field," Nucl. Instr. and Methods 4 (1959).
7. K. N. Mukhin, et al., "A Bubble Chamber in a Pulsed Magnetic Field," International Conference on High-Energy Accelerators and Instrumentation, CERN, 1959, pp. 514-19.
8. J. M. Toth, Jr., Advances in Cryogenic Engineering, Vol. 9, p. 537 (1963).
9. J. M. Toth, Jr., Advances in Cryogenic Engineering, Vol. 10, p. 134 (1964).
10. D. W. Chamberlin, Advances in Cryogenic Engineering, Vol. 10, p. 117 (1964).
11. S. Timoshenko and S. Woinowsky-Krieger, Theory of Plates and Shells, McGraw-Hill (1959).
12. V. V. Novozhilov, The Theory of Thin Shells, Nordhoff (1959).
13. H. Brechna, "Effect of nuclear radiation on magnet insulation in high energy accelerators," SLAC Report No. 40, Stanford Linear Accelerator Center, Stanford University, Stanford, California (1965).

14. H. Brechna, "Mechanical and thermal properties of thick wall filament wound chambers," SLAC Internal Report, Stanford Linear Accelerator Center, Stanford University, Stanford, California, (1964).

15. J. Hertz and J. F. Haskins, Advances in Cryogenic Engineering, Vol. 10, p. 163 (1964).

LIST OF FIGURES

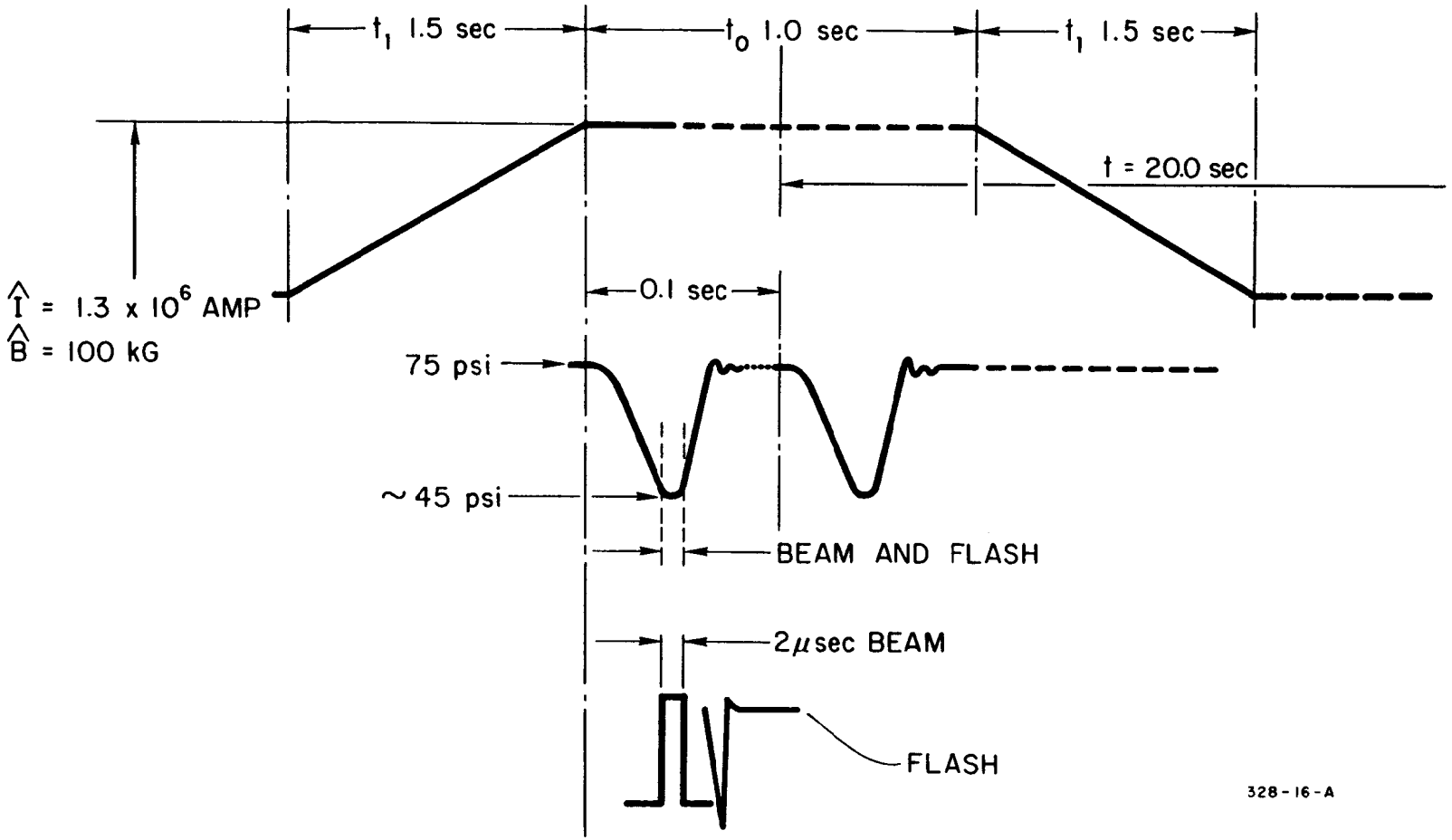
t_1 1.5 sec
t_o 1.0 sec
t_1 1.5 sec
t = 20.0 sec
$\hat{I}$ = 1.3 x 10^6 AMP
$\hat{B}$ = 100 kG
0.1 sec
75 psi
~45 psi
BEAM AND FLASH
2μsec BEAM
FLASH
328-16-A

FIG. 1

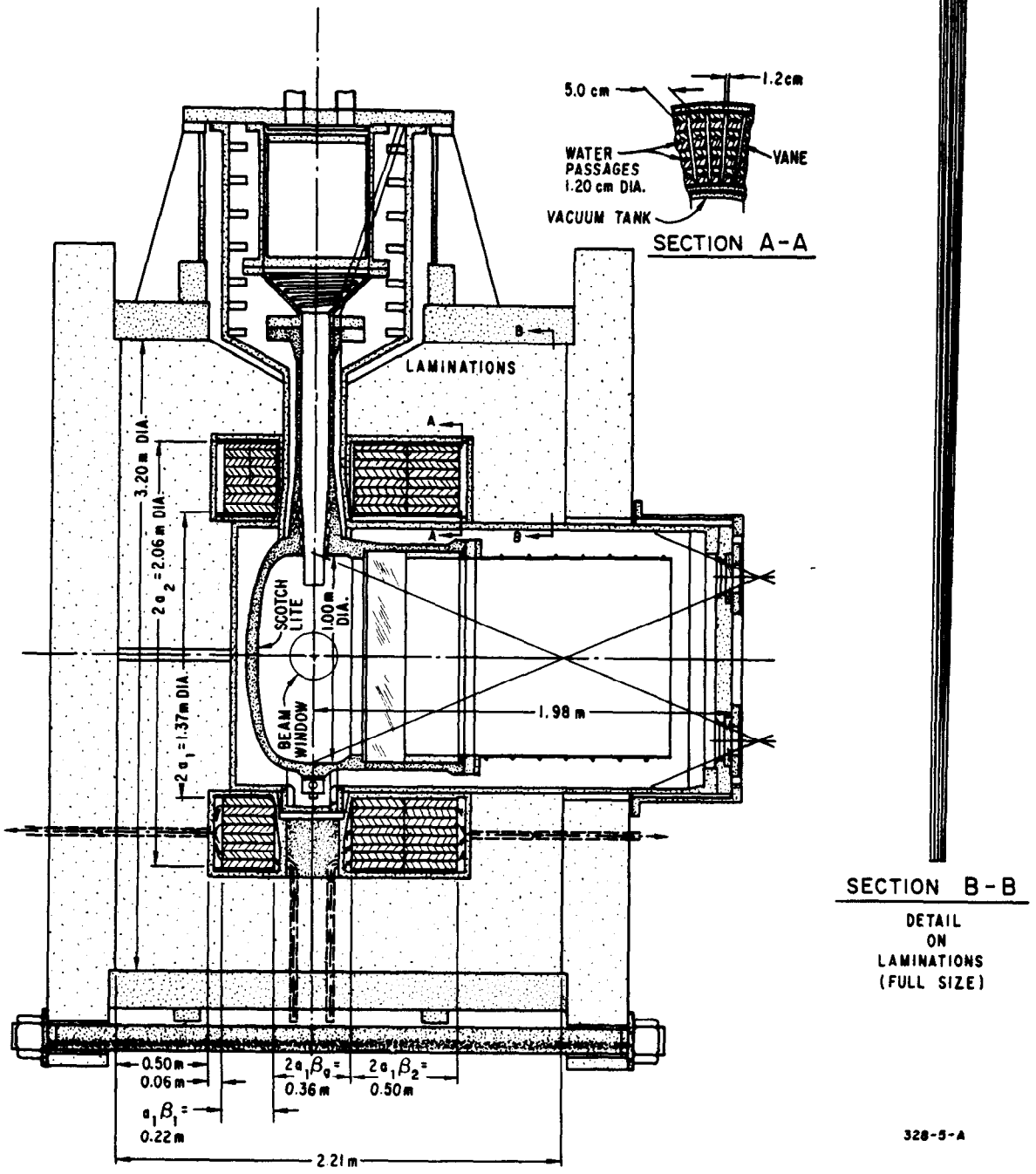
5.0 cm
1.2cm
WATER PASSAGES 1.20 cm DIA.
VANE
VACUUM TANK
SECTION A-A
LAMINATIONS
B
A
3.20 m DIA.
2a2 = 2.06 m DIA.
2a1 = 1.37m DIA.
SCOTCH LITE
1.00m DIA.
BEAM WINDOW
1.98 m
0.50m
0.06 m
2a1β0 = 0.36 m
2a1β2 = 0.50m
a1β1 = 0.22m
2.21m
SECTION B-B
DETAIL ON LAMINATIONS (FULL SIZE)
328-5-A

FIG. 2

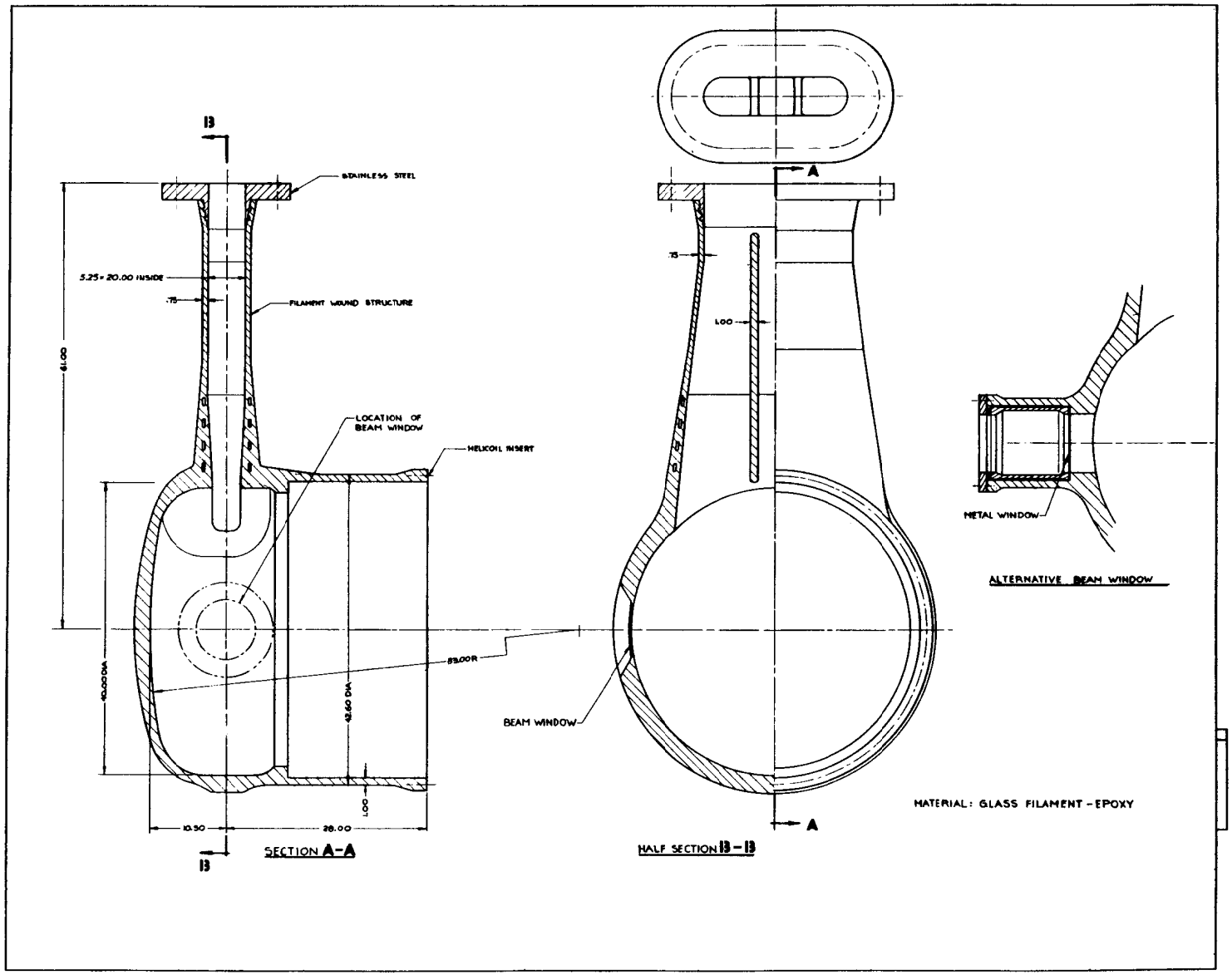

328-13-A

FIG. 3a

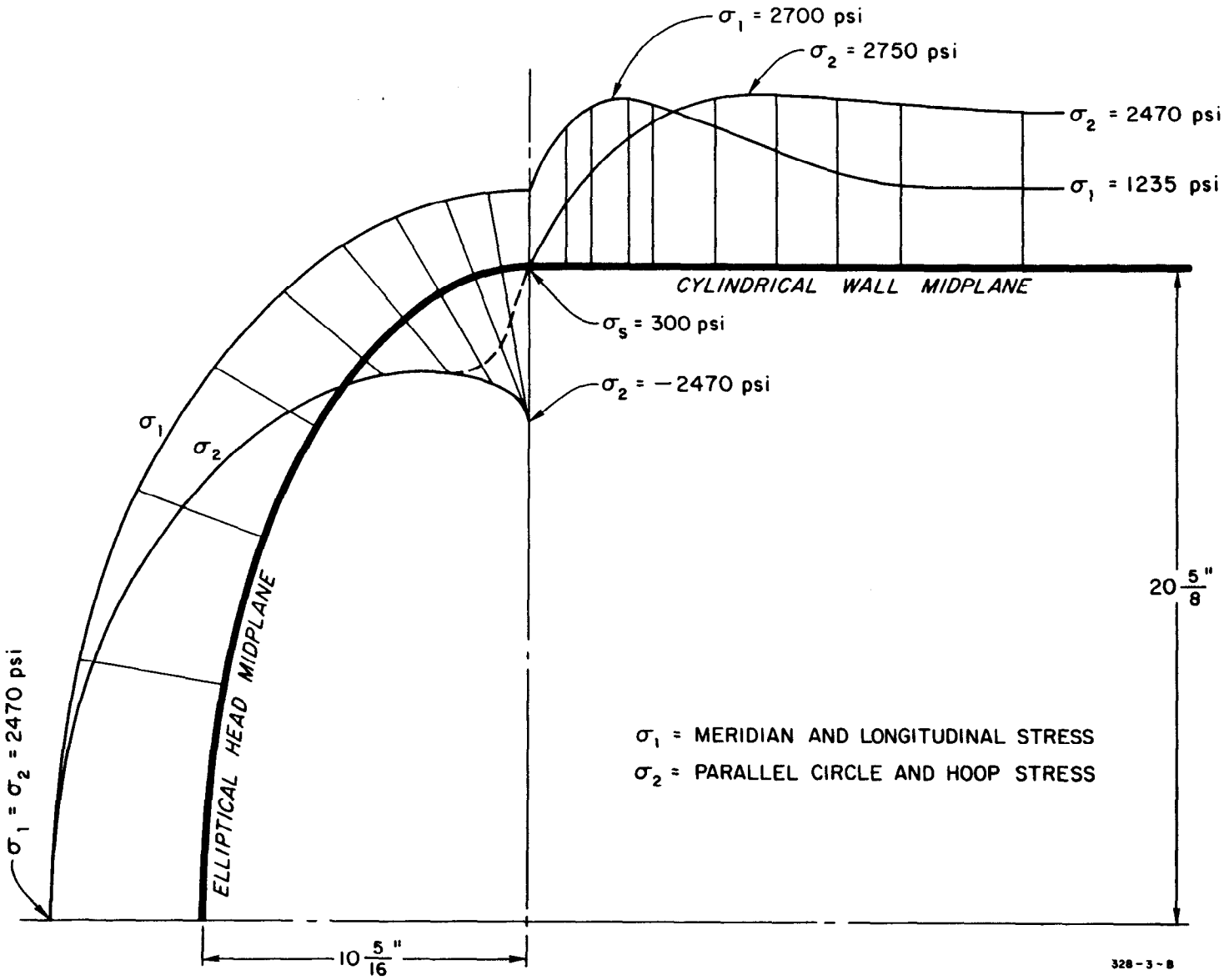
σ_1 = 2700 psi
σ_2 = 2750 psi
σ_2 = 2470 psi
σ_1 = 1235 psi
CYLINDRICAL WALL MIDPLANE
σ_s = 300 psi
σ_2 = −2470 psi
σ_1
σ_2
ELLIPTICAL HEAD MIDPLANE
$\sigma_1 = \sigma_2$ = 2470 psi
$20\frac{5}{8}$"
σ_1 = MERIDIAN AND LONGITUDINAL STRESS
σ_2 = PARALLEL CIRCLE AND HOOP STRESS
$10\frac{5}{16}$"
328-3-8

FIG. 3b

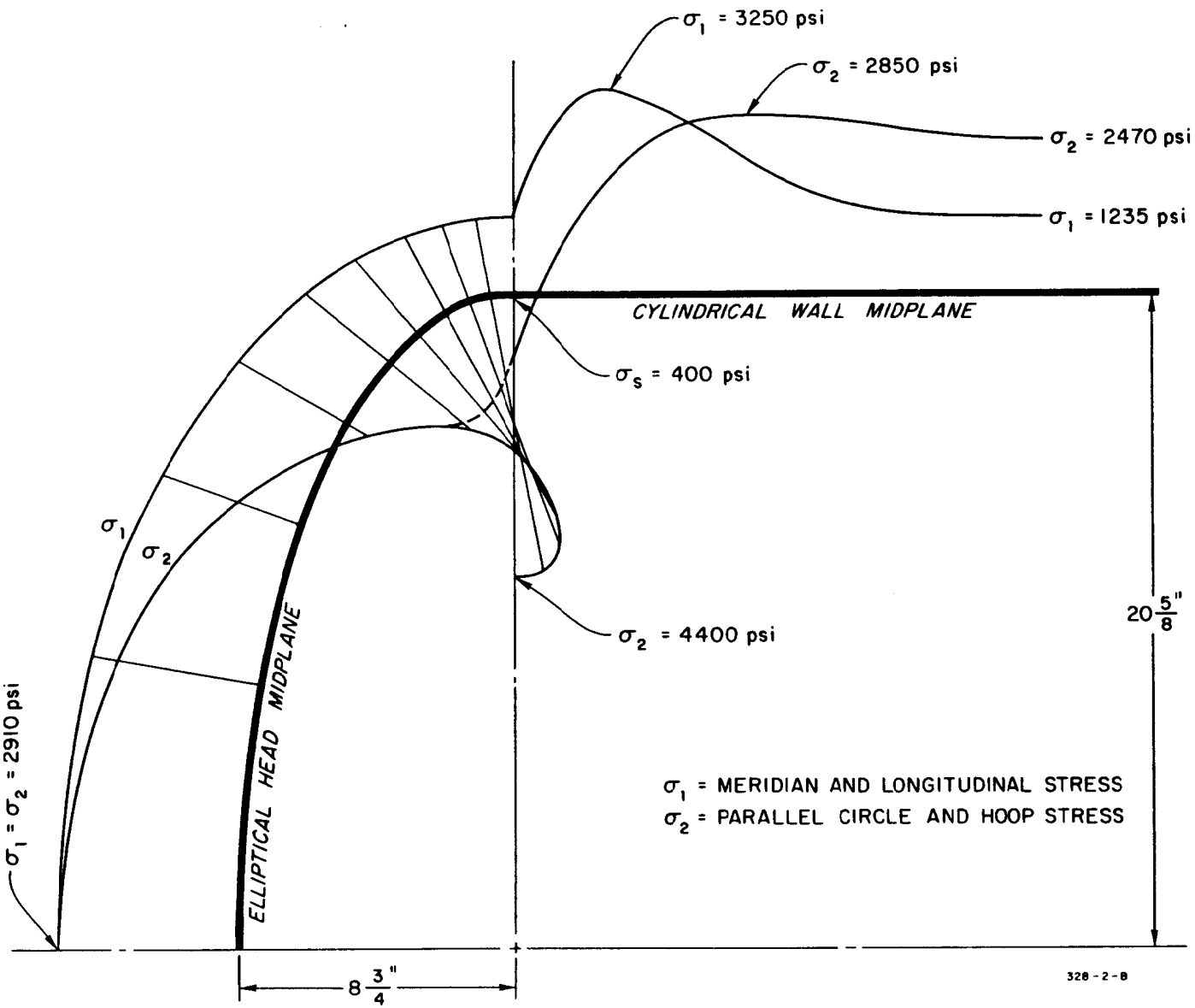
σ_1 = 3250 psi
σ_2 = 2850 psi
σ_2 = 2470 psi
σ_1 = 1235 psi
CYLINDRICAL WALL MIDPLANE
σ_s = 400 psi
σ_1
σ_2
ELLIPTICAL HEAD MIDPLANE
σ_2 = 4400 psi
$20\frac{5}{8}$"
$\sigma_1 = \sigma_2$ = 2910 psi
σ_1 = MERIDIAN AND LONGITUDINAL STRESS
σ_2 = PARALLEL CIRCLE AND HOOP STRESS
$8\frac{3}{4}$"
328-2-8

FIG. 3c

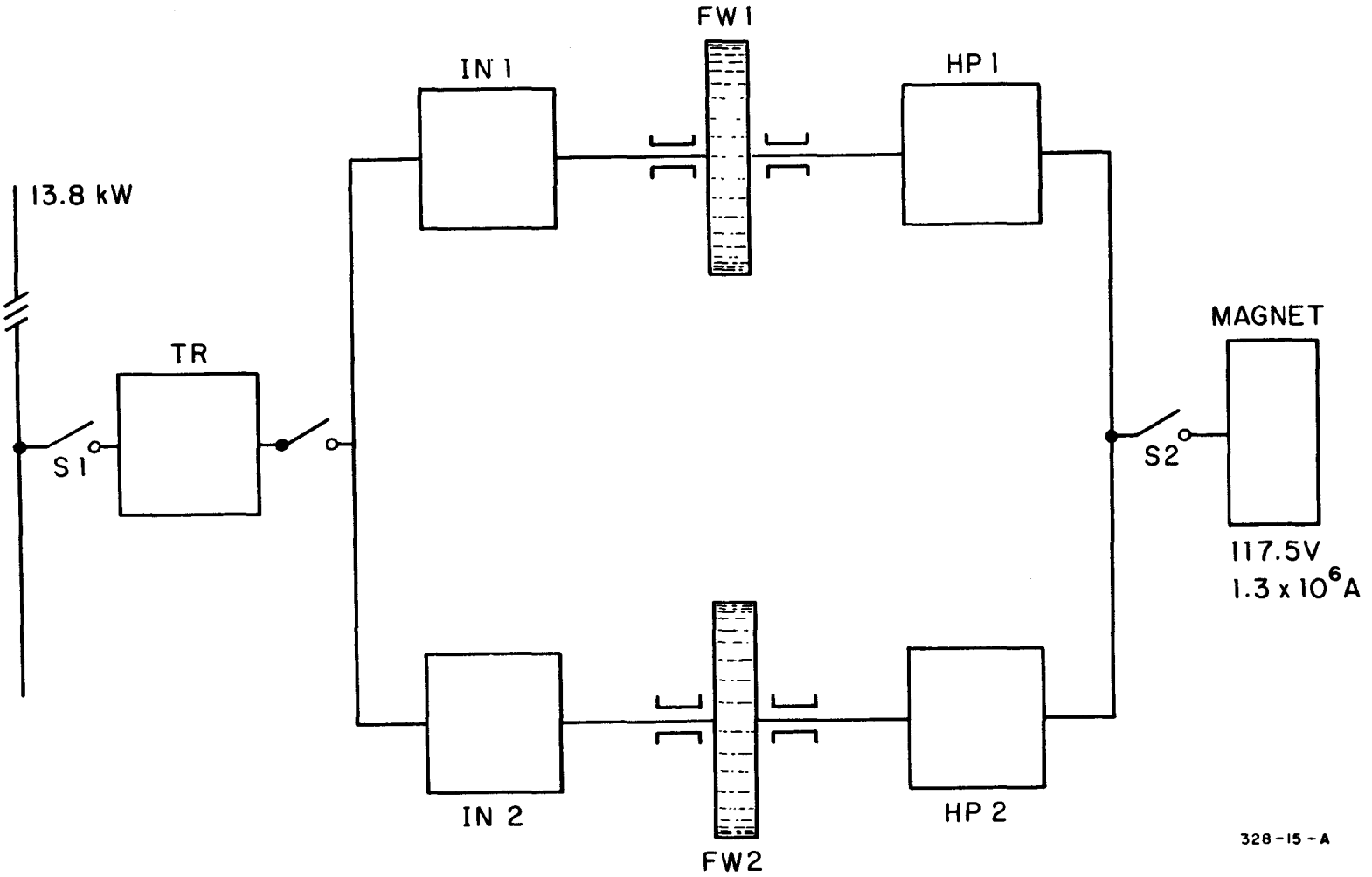
FW1
IN 1
HP 1
13.8 kW
TR
MAGNET
S1
S2
117.5V
1.3 x 10^6 A
IN 2
HP 2
FW2
328-15-A

FIG. 4

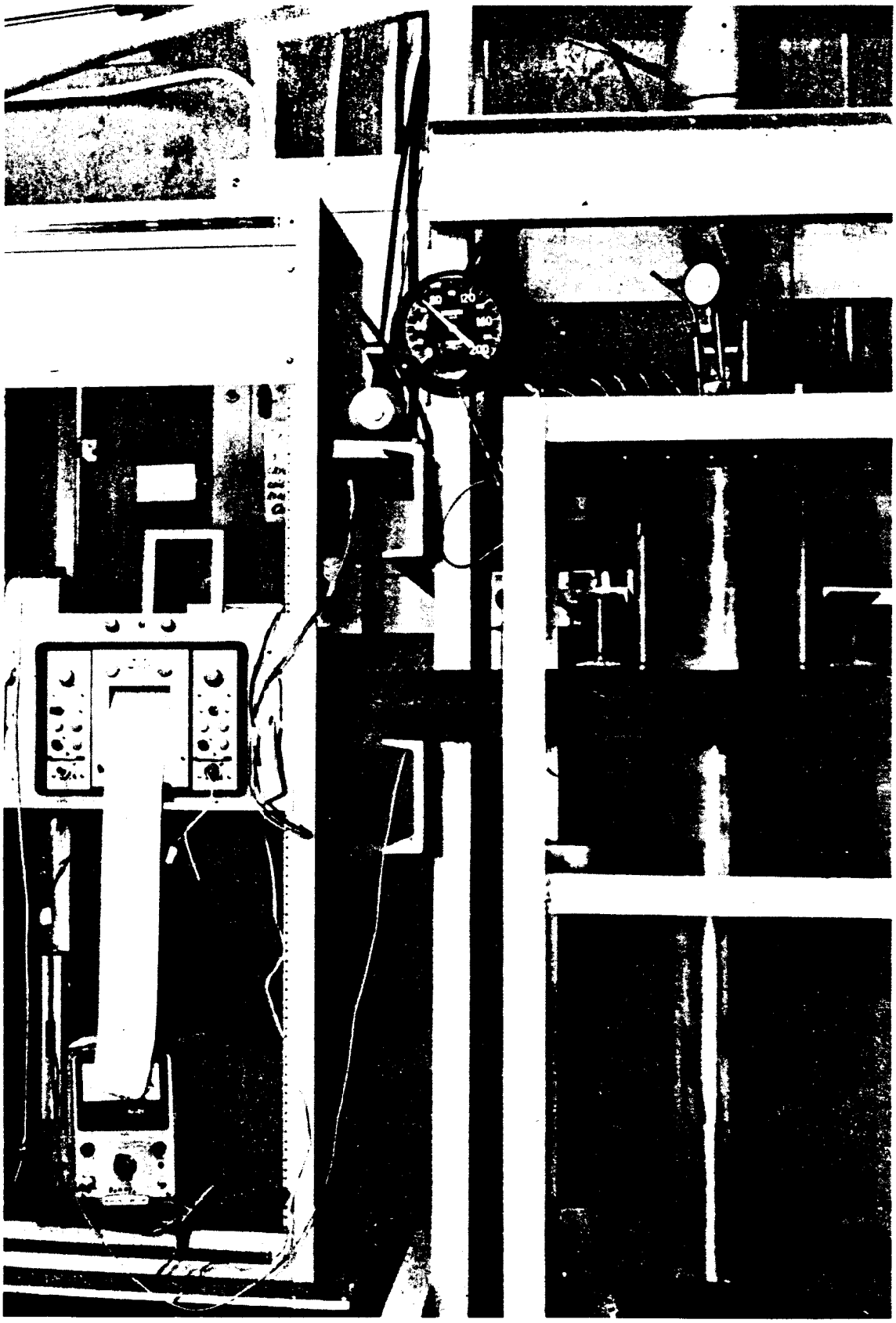

328 - 19 - A

FIG. 5a

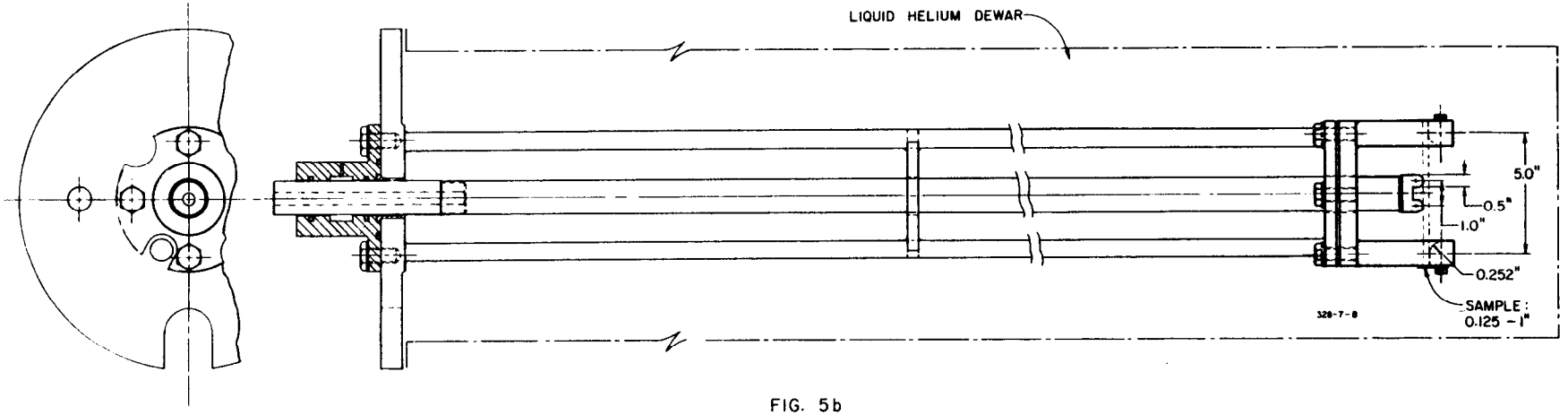

FIG. 5b

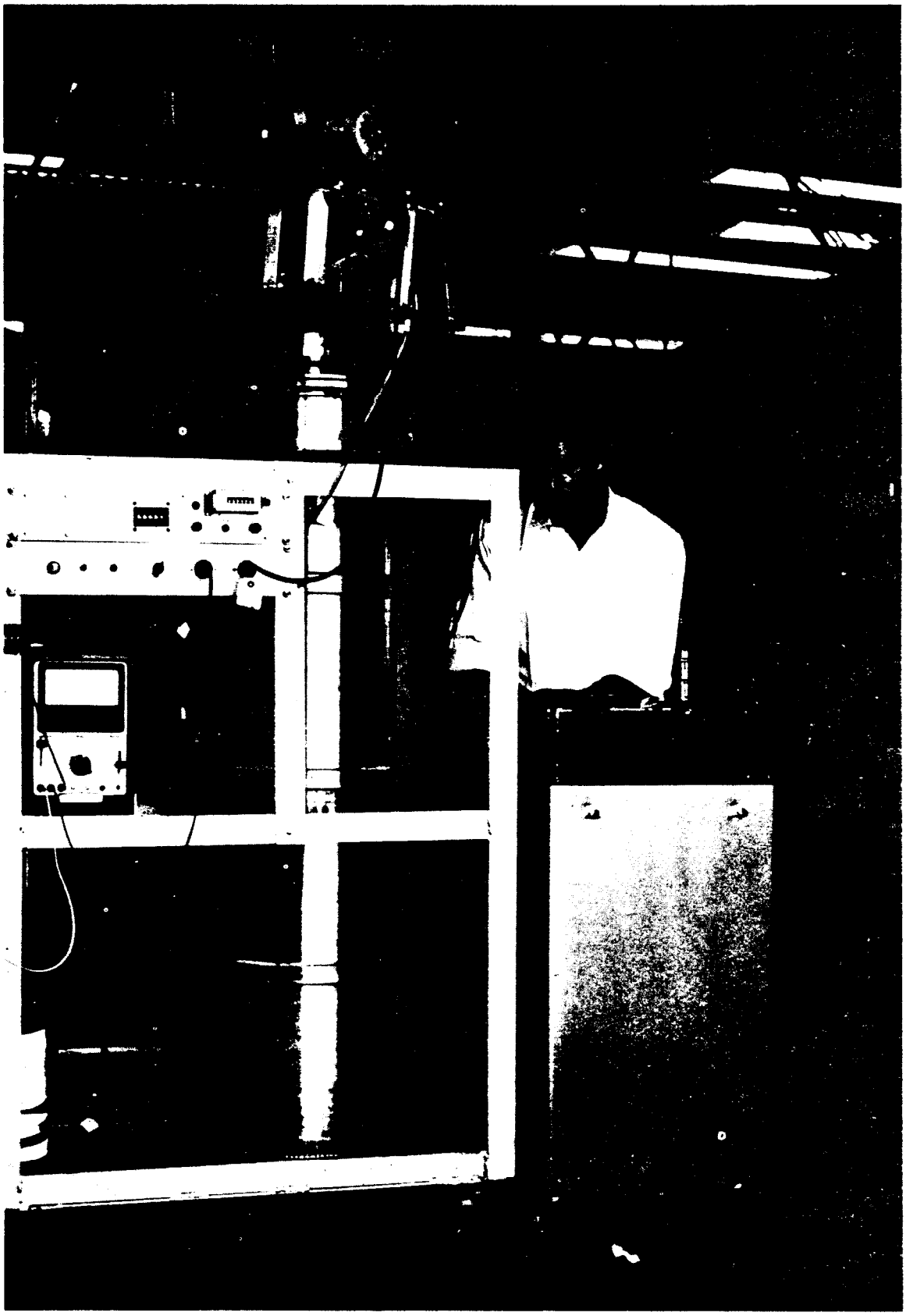

328-20-A

FIG. 6a

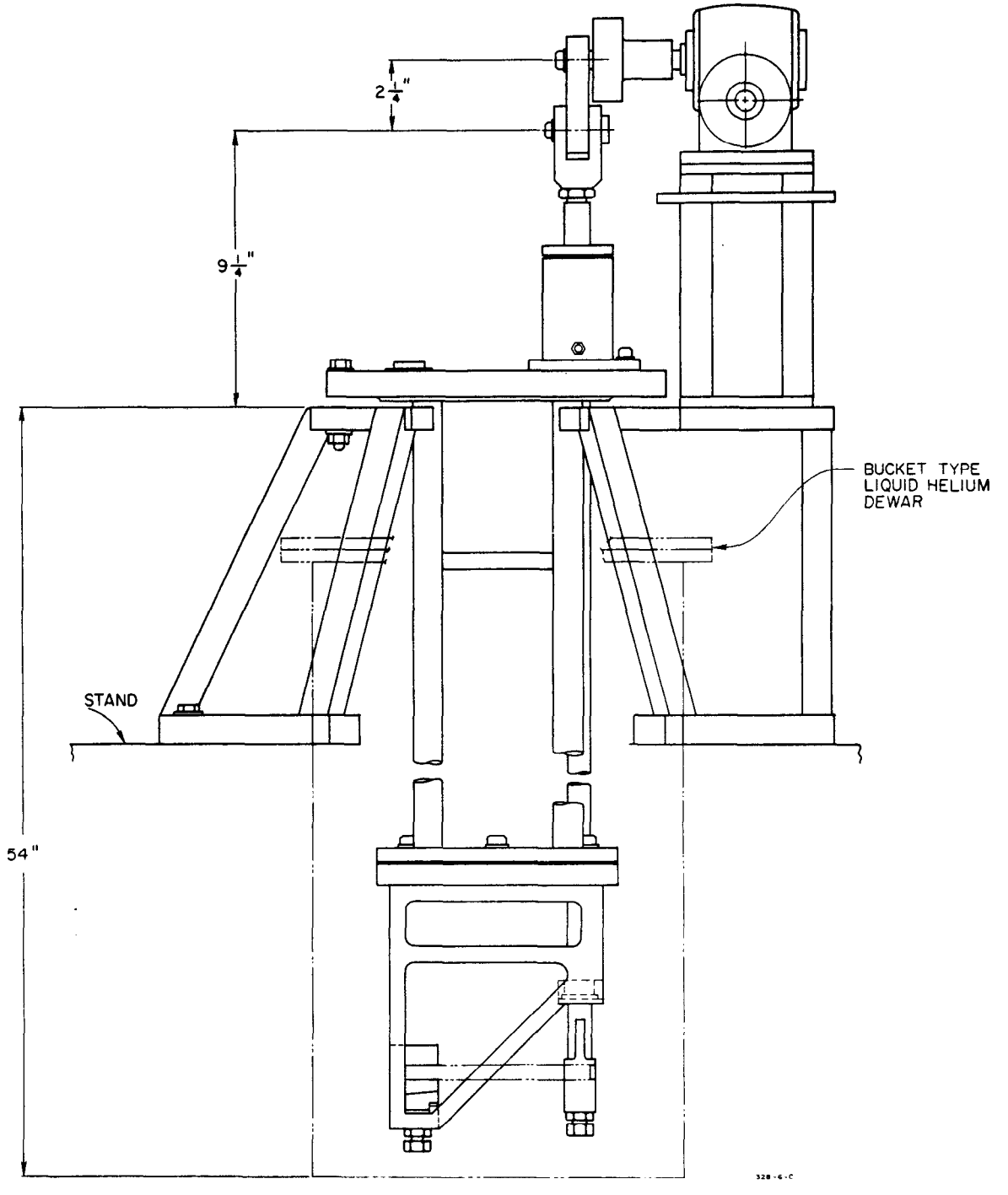

FIG. 6b

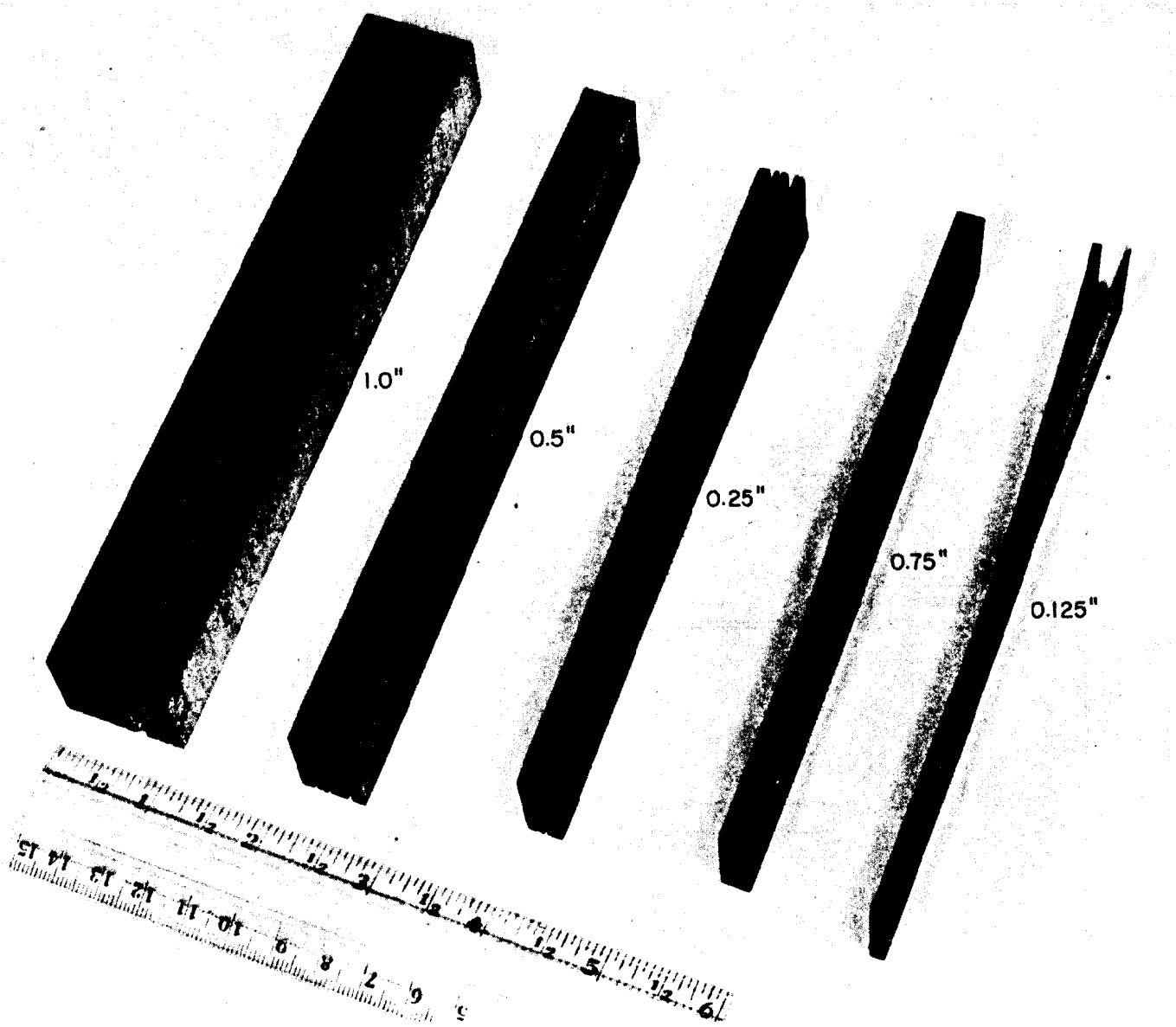

FIG. 7

328-9-A

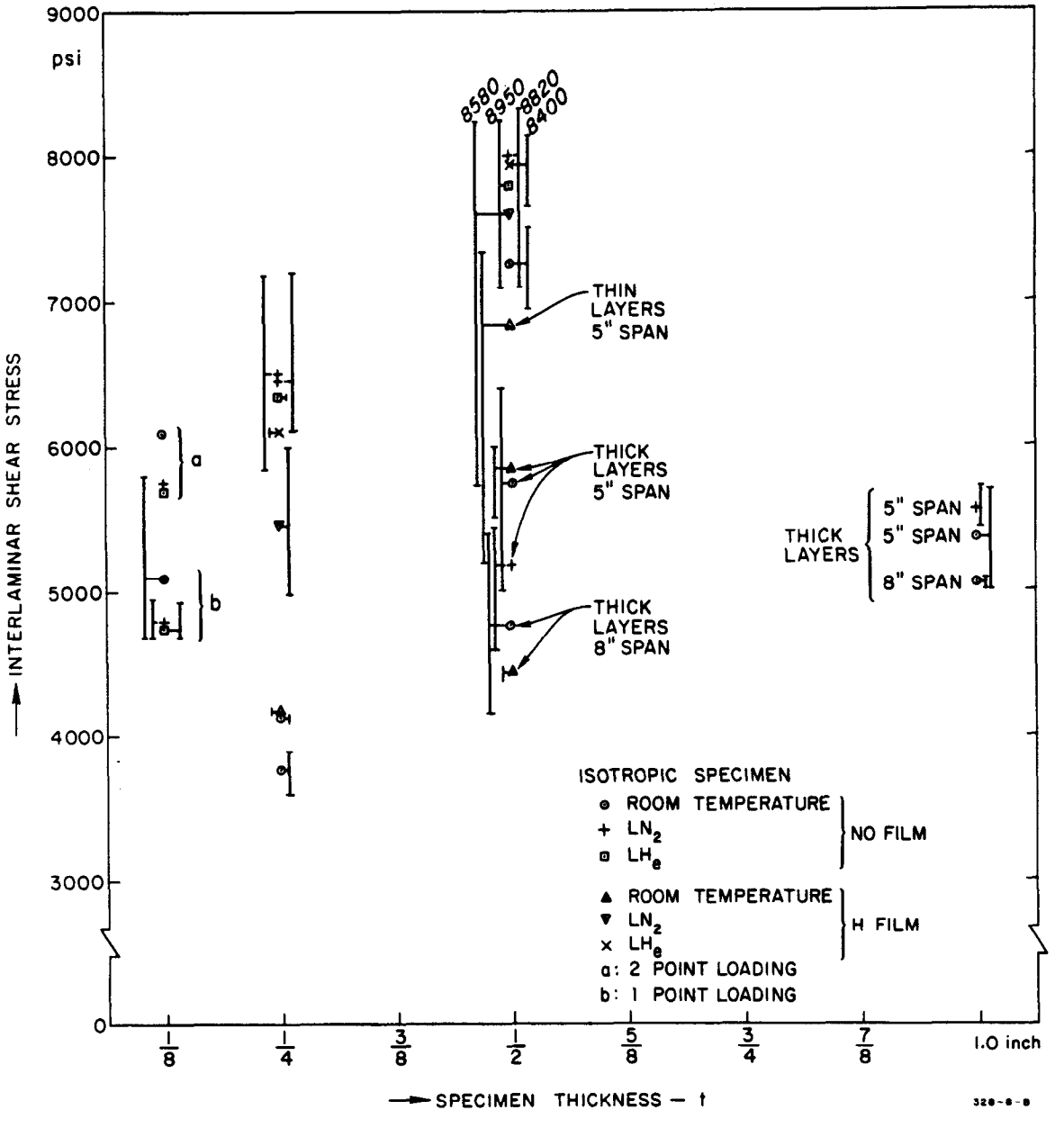
9000
psi
8000
7000
6000
5000
4000
3000
0
INTERLAMINAR SHEAR STRESS
8580
8950
8820
8400
THIN LAYERS 5" SPAN
THICK LAYERS 5" SPAN
THICK LAYERS 8" SPAN
a
b
THICK LAYERS
5" SPAN
5" SPAN
8" SPAN
ISOTROPIC SPECIMEN
ROOM TEMPERATURE
LN2
LHe
NO FILM
ROOM TEMPERATURE
LN2
LHe
H FILM
a: 2 POINT LOADING
b: 1 POINT LOADING
1/8
1/4
3/8
1/2
5/8
3/4
7/8
1.0 inch
SPECIMEN THICKNESS — t

FIG. 8

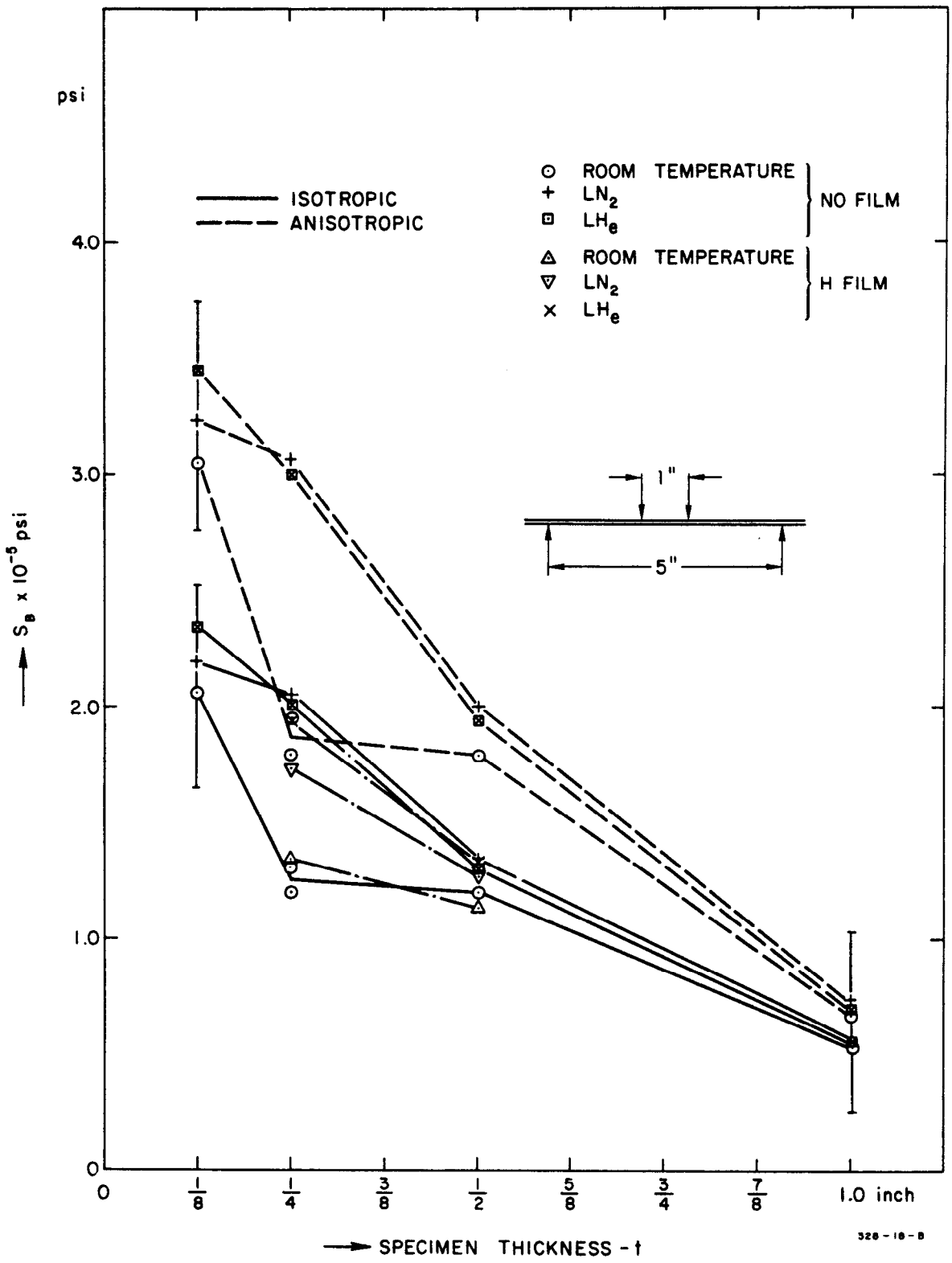
psi
ISOTROPIC
ANISOTROPIC
ROOM TEMPERATURE
LN2
LHe
NO FILM
ROOM TEMPERATURE
LN2
LHe
H FILM
1"
5"
4.0
3.0
2.0
1.0
0
$S_B \times 10^{-5}$ psi
0
1/8
1/4
3/8
1/2
5/8
3/4
7/8
1.0 inch
SPECIMEN THICKNESS - t
328-18-8

FIG. 9

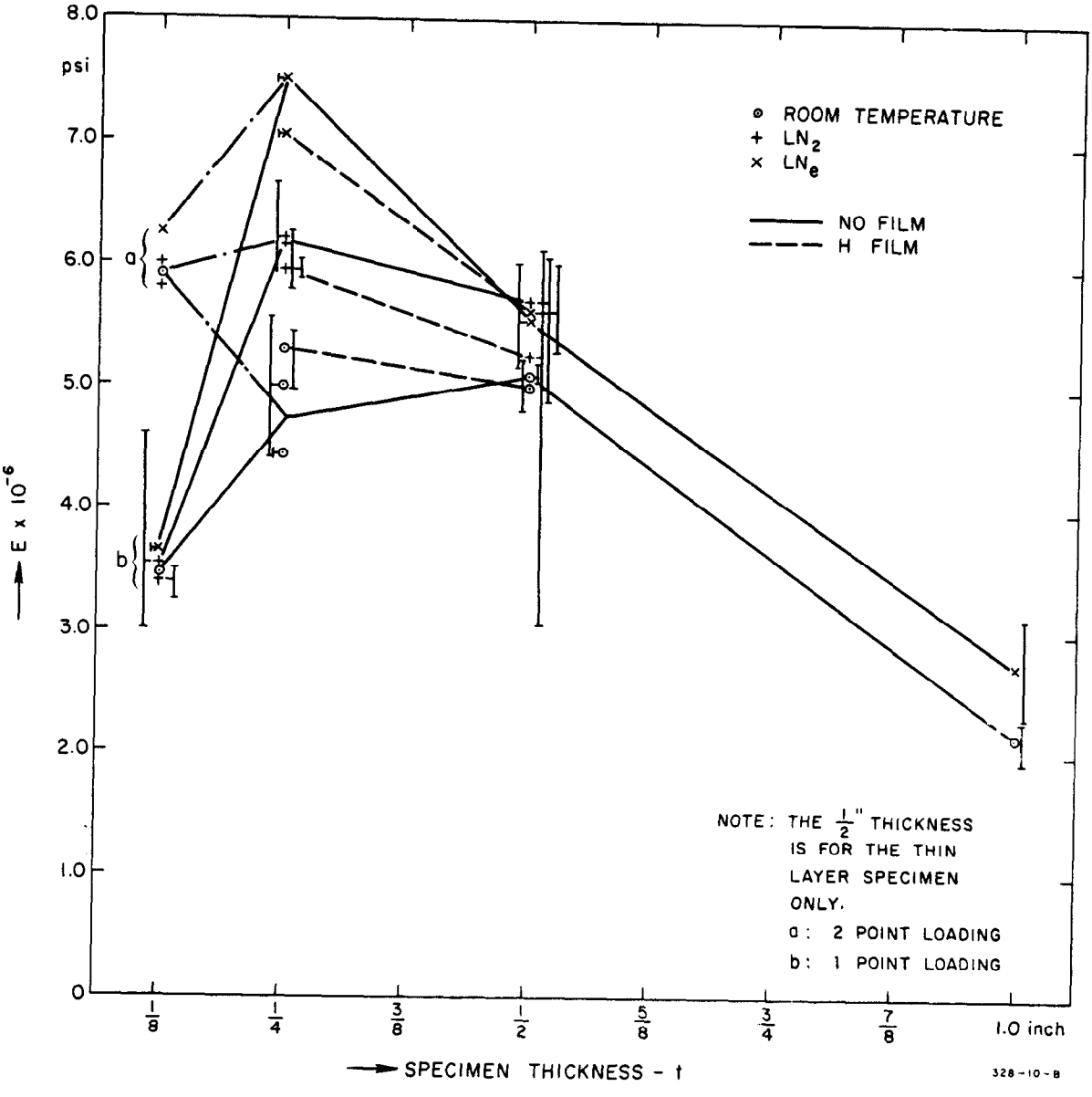
8.0
psi
7.0
6.0
5.0
4.0
3.0
2.0
1.0
0
E x 10⁻⁶
a
b
⊙ ROOM TEMPERATURE
+ LN2
× LNe
NO FILM
H FILM
NOTE: THE 1/2" THICKNESS IS FOR THE THIN LAYER SPECIMEN ONLY.
a: 2 POINT LOADING
b: 1 POINT LOADING
1/8
1/4
3/8
1/2
5/8
3/4
7/8
1.0 inch
SPECIMEN THICKNESS - t
328-10-B

FIG. 10

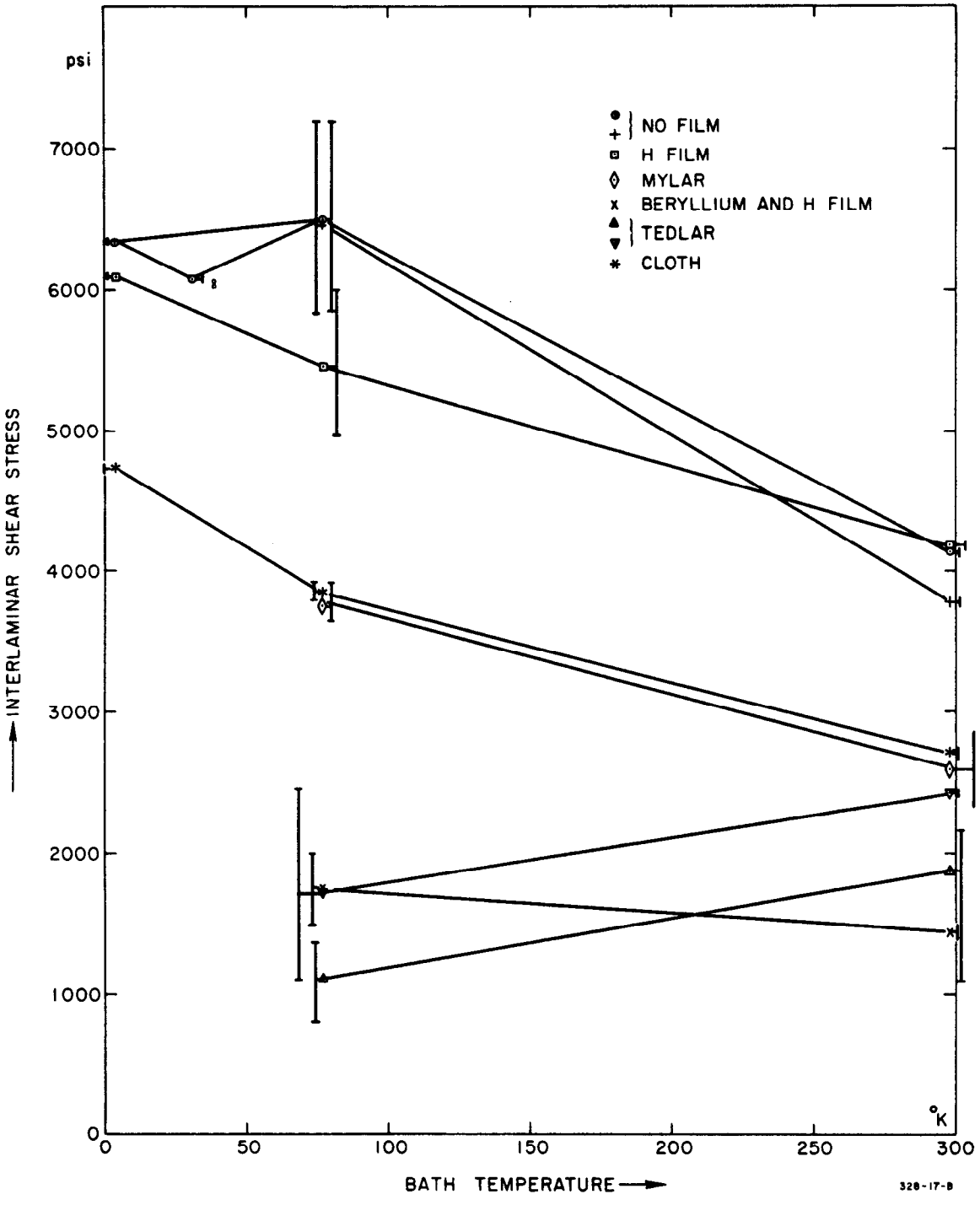
psi
7000
6000
5000
4000
3000
2000
1000
0
INTERLAMINAR SHEAR STRESS
NO FILM
H FILM
MYLAR
BERYLLIUM AND H FILM
TEDLAR
CLOTH
°K
0
50
100
150
200
250
300
BATH TEMPERATURE
328-17-B

FIG. 11

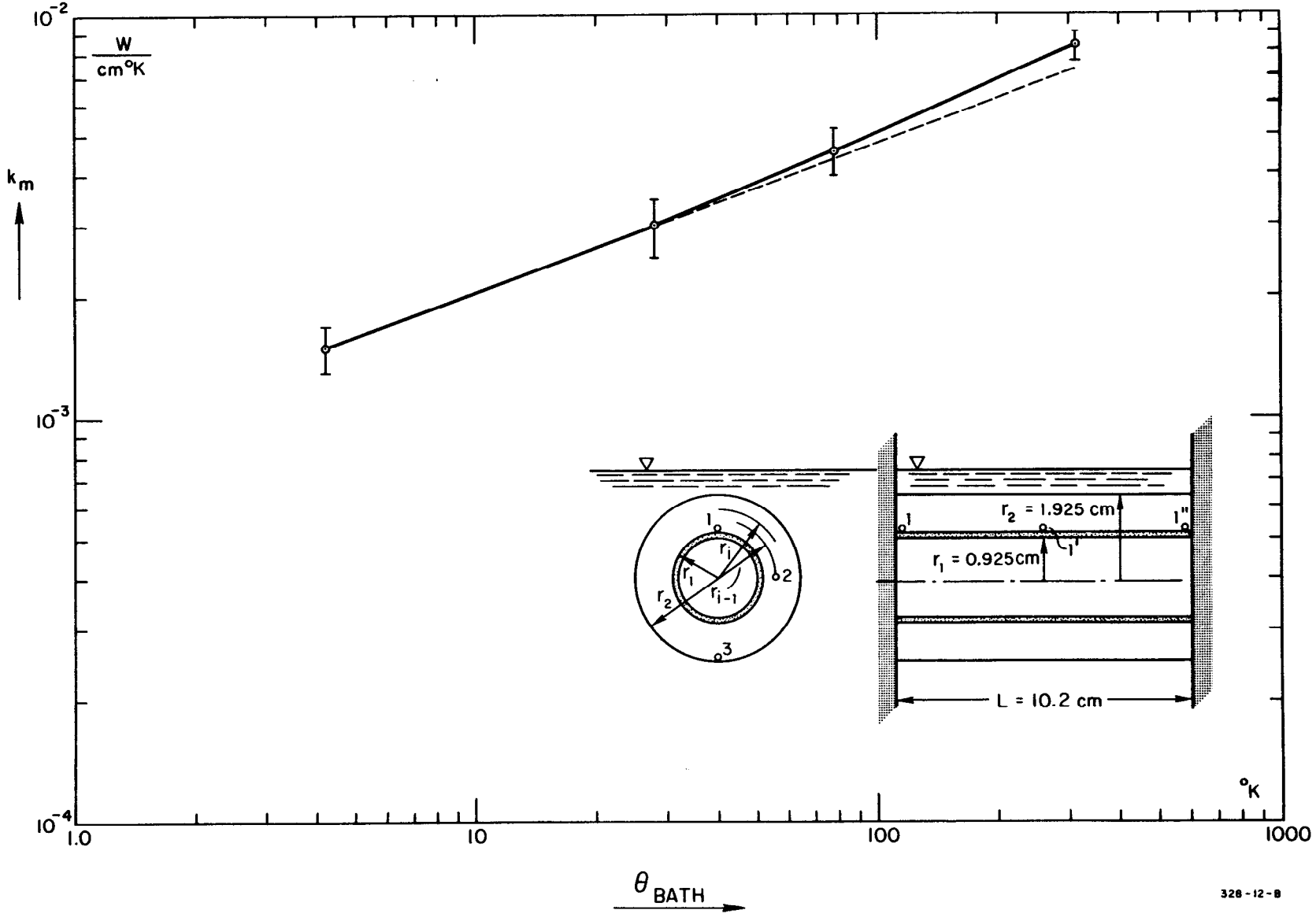
10^{-2}
W
cm°K
k_m
10^{-3}
10^{-4}
1.0
10
100
1000
°K
θ_{BATH}
r_2 = 1.925 cm
r_1 = 0.925cm
L = 10.2 cm
1
1'
1"
2
3
r_i
r_{i-1}
328-12-B

FIG. 12

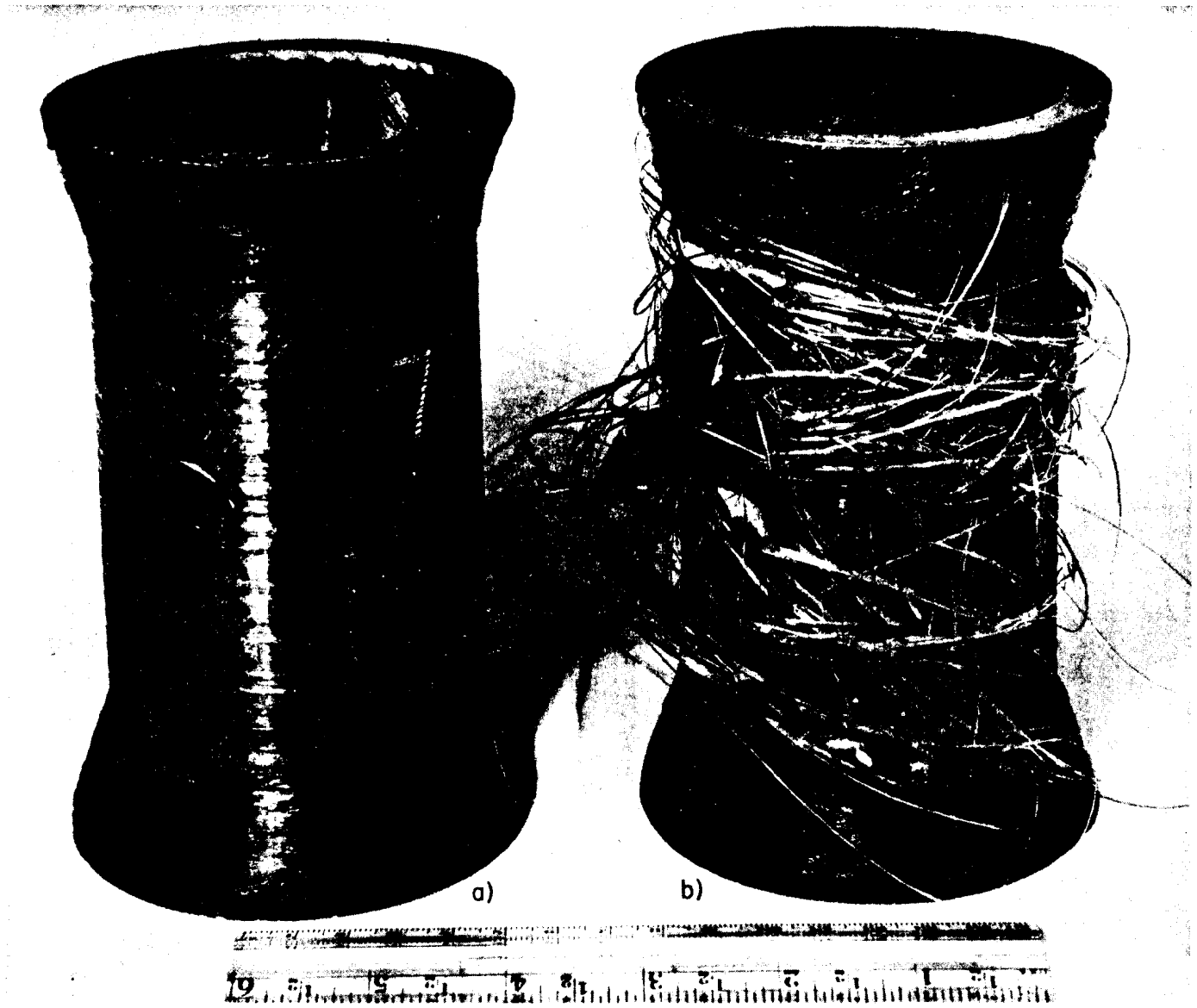

FIG. 13

328-14-A

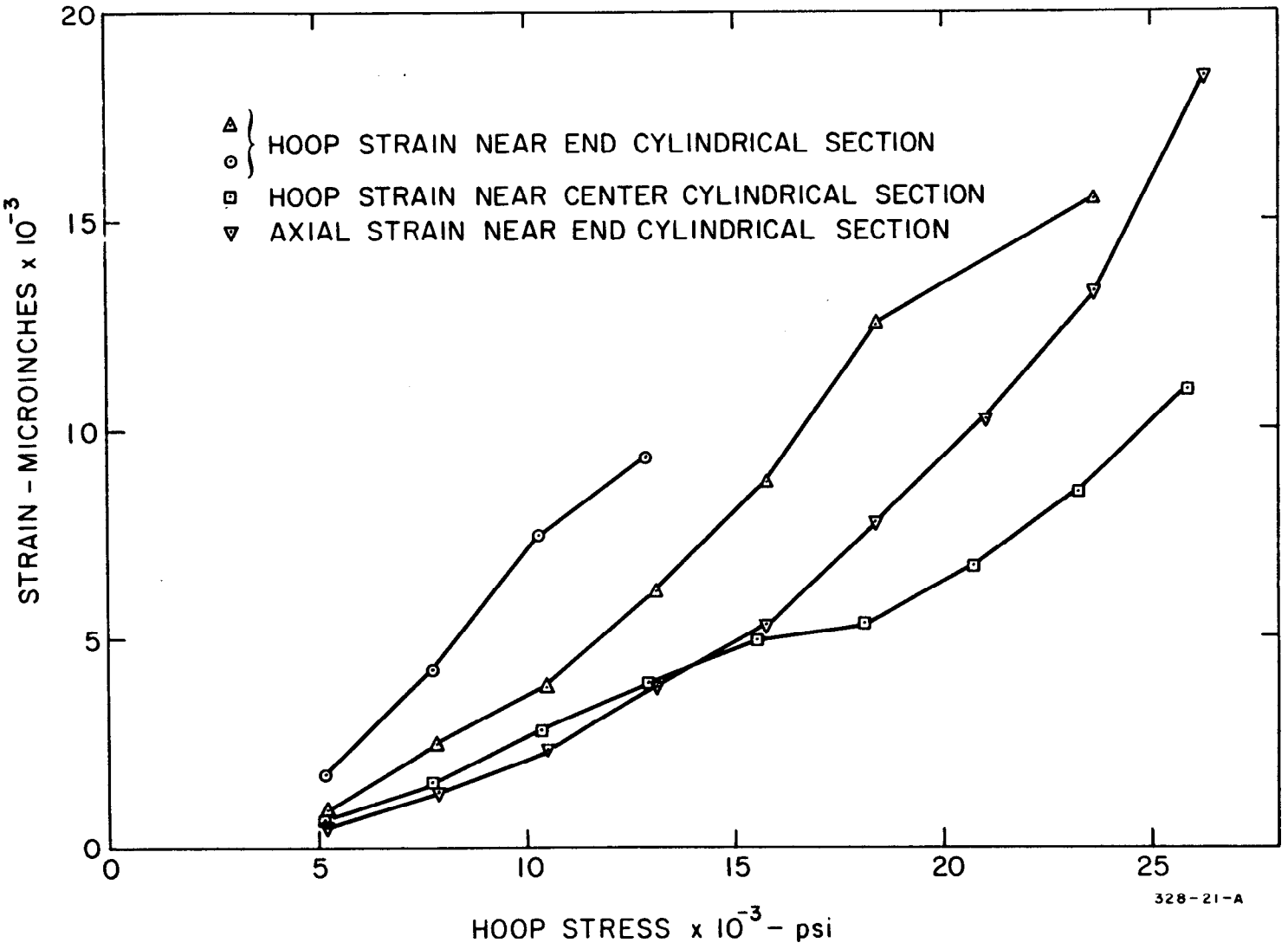
HOOP STRAIN NEAR END CYLINDRICAL SECTION
HOOP STRAIN NEAR CENTER CYLINDRICAL SECTION
AXIAL STRAIN NEAR END CYLINDRICAL SECTION
STRAIN - MICROINCHES x 10^-3
HOOP STRESS x 10^-3 - psi
0
5
10
15
20
25
328-21-A

FIG. 14

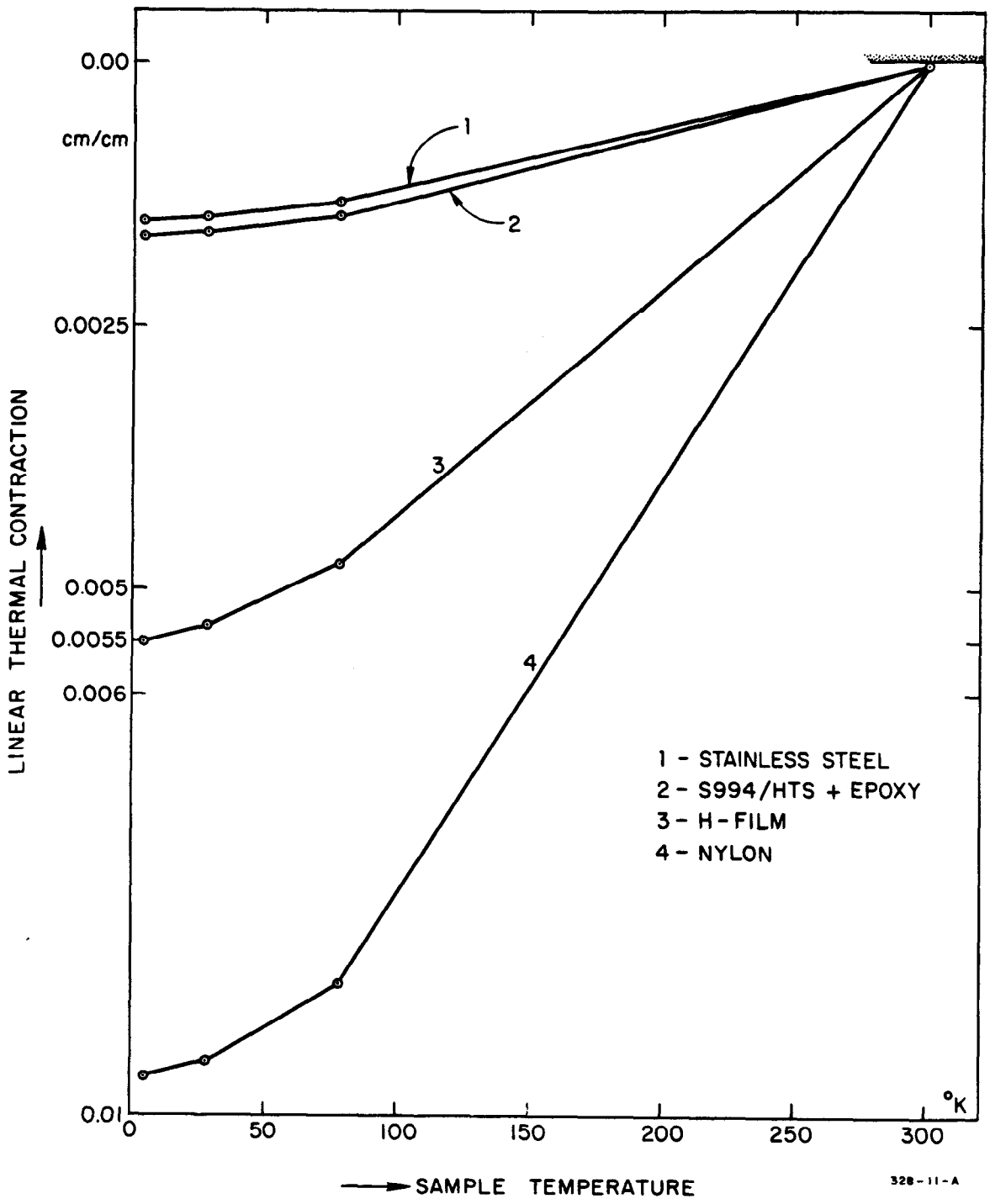
0.00
cm/cm
0.0025
0.005
0.0055
0.006
0.01
LINEAR THERMAL CONTRACTION
1
2
3
4
1 - STAINLESS STEEL
2 - S994/HTS + EPOXY
3 - H-FILM
4 - NYLON
0
50
100
150
200
250
300
°K
SAMPLE TEMPERATURE
328-11-A

FIG. 15